HHS Public Access

Author manuscript

J Comp Neurol. Author manuscript; available in PMC 2017 December 07.

Published in final edited form as:

J Comp Neurol. 2017 October 15; 525(15): 3286–3311. doi:10.1002/cne.24278.

Cerebellins Are Differentially Expressed in Selective Subsets of Neurons Throughout the Brain

Erica Seigneur and **Thomas C. Südhof**

Department of Molecular & Cellular Physiology and Howard Hughes Medical Institute, Stanford University Medical School, 265 Campus Drive, SIM1 Bldg, Room G1021, Stanford, California 94305, USA

Abstract

Cerebellins are secreted hexameric proteins that form tripartite complexes with the presynaptic cell-adhesion molecules neurexins or 'deleted-in-colorectal-cancer' (DCC), and the postsynaptic glutamate-receptor-related proteins GluD1 and GluD2. These tripartite complexes are thought to regulate synapses. However, cerebellins are expressed in multiple isoforms whose relative distributions and overall functions are not understood. Three of the four cerebellins, Cbln1, Cbln2, and Cbln4, autonomously assemble into homohexamers, whereas the Cbln3 requires Cbln1 for assembly and secretion. Here, we show that Cbln1, Cbln2, and Cbln4 are abundantly expressed in nearly all brain regions, but exhibit strikingly different expression patterns and developmental dynamics. Using newly generated knockin reporter mice for Cbln2 and Cbln4, we find that Cbln2 and Cbln4 are not universally expressed in all neurons, but only in specific subsets of neurons. For example, Cbln2 and Cbln4 are broadly expressed in largely non-overlapping subpopulations of excitatory cortical neurons, but only sparse expression was observed in excitatory hippocampal neurons of the CA1- or CA3-region. Similarly, Cbln2 and Cbln4 are selectively expressed, respectively, in inhibitory interneurons and excitatory mitral projection neurons of the main olfactory bulb; here, these two classes of neurons form dendrodendritic reciprocal synapses with each other. A few brain regions, such as the nucleus of the lateral olfactory tract, exhibit astoundingly high Cbln2 expression levels. Viewed together, our data show that cerebellins are abundantly expressed in relatively small subsets of neurons, suggesting specific roles restricted to subsets of synapses.

Keywords

Cerebellin; neurexin; neuronal cell adhesion; molecules; protein isoforms; synapses; synaptogenesis; RRID: AB_476894; RRID: AB_94259; RRID: AB_2067919; RRID: AB_10000240; RRID: AB_477329; RRID: AB_572264; RRID: AB_2201528

INTRODUCTION

Cerebellins are secreted glycoproteins that belong to the C1q and tumor necrosis factor (TNF) superfamily (Kishore et al., 2004). Cerebellins function as *trans*-synaptic cell-

Please address correspondence to T.C.S. at tcs1@stanford.edu.

adhesion molecules that critically contribute to the formation and/or function of synapses (Ito-Ishida et al., 2008; Uemura et al., 2010; Lee et al., 2012). In genetic studies, mutations in cerebellins and their presynaptic neurexin receptors are associated with autism spectrum disorders (ASDs), schizophrenia, Tourette syndrome, and various other neurological diseases (reviewed in Südhof, 2008; Clarke et al., 2012; Bourgeron, 2015), but the biological implications of these associations remain unclear. Vertebrates express four cerebellins (Cbln1-4) that are produced throughout the brain (Miura et al., 2006; Wei et al., 2012; Cagle and Honig, 2014). Cbln1, Cbln2, and Cbln4 assemble into autonomous homo-hexamers in the secretory pathway, and are thus independent of each other (even though sometimes co-expressed; see below), whereas Cbln3 is unable to assemble into homo-hexamers and requires co-expression of Cbln1 for function (Pang et al., 2000).

Presynaptically, Cbln1 and Cbln2 bind with high affinity to α- and β-neurexins containing an insert in splice-site #4, but not to α- and β-neurexins lacking an insert in splice site #4 (Uemura et al., 2010; Matsuda and Yuzaki, 2011). Cbln4 only weakly binds to neurexins, but instead binds with high affinity to DCC (‘deleted in colorectal cancer’) and neogenin-1, which are homologous cell-adhesion molecules (Wei et al., 2012; Haddick et al., 2014). Postsynaptically, Cbln1, Cbln2, and Cbln4 bind to GluD1 and GluD2, two closely related proteins that resemble ionotropic glutamate receptors but do not appear to have a glutamate receptor function (Matsuda et al., 2010; Ryu et al., 2012). Cerebellin binding to neurexins and to GluDs is mediated by their N-terminal stalk and C-terminal C1q-domain sequences, respectively; simultaneously binding to both ligands results in a tripartite complex that is thought to span the synaptic cleft, and that is capable of bidirectional synapse induction in the artificial synapse formation assay (Lee et al., 2012).

In the cerebellum, Cbln1 is secreted from presynaptic granule cells and functions as a *trans*-synaptic organizer of parallel fiber-Purkinje cell synapses by binding to presynaptic neurexins and postsynaptic GluDs. Cbln1 KO mice exhibit cerebellar synapse loss, are ataxic, and exhibit impaired motor learning (Hirai et al., 2005; Rong et al., 2012). Interestingly, the Cbln1 KO caused a different phenotype in striatum (Kusnoor et al., 2010). Here, Cbln1-deficient thalamic axons exhibited an increase in synaptic spine density instead of a synapse loss, suggesting that cerebellins may in general perform a signaling function instead of a synapse-formation function. Moreover, Cbln1 was shown to be essential for hippocampal learning by an unknown mechanism (Otsuka et al., 2016). Although our understanding of Cbln1 function is thus incomplete, even less is known about the expression patterns and functions of Cbln2 and Cbln4. Cbln2 and Cbln4 KO mice were reported (Rong et al., 2012; Wei et al., 2012; Haddick et al., 2014). However, these previous studies largely focused on the function of Cbln2 or Cbln4 in the cerebellum or in axon guidance, and there is currently no assessment of their overall functions or expression.

In the present study, we generated knockin reporter mice to systematically map the precise expression patterns of Cbln2 and Cbln4 throughout the brain as a first step to analyzing the overall role of this enigmatic protein family. Our data demonstrate an amazingly diverse and abundant expression pattern for cerebellins, and provides an essential framework for understanding the function of these proteins.

METHODS

Mouse handling and husbandry

All experiments were performed with male and female young adult, C57/Bl6/SV129 hybrid mice. All animal procedures conformed to National Institutes of Health's *Guidelines for the Care and Use of Laboratory Animals* and were approved by the Stanford University Administrative Panel on Laboratory Animal Care.

Generation of knock-in (KI) Cbln2 and Cbln4 reporter mice

Floxed IRES-mVenus-IRES-tdTomato reporter mice for Cbln2 and Cbln4 were constructed by homologous recombination using recombineering techniques (Liu et al., 2003). A genomic clone containing exons 1-3 of the Cbln2 or Cbln4 gene was isolated from a bacterial artificial chromosome (BAC) DNA library. The first *loxP* site with BamHI was inserted into intron 2, between exons 1 and 2. Exon 2-3 then functioned as the promoter sequence driving the expression of an IRES-mVenus, which was followed by a neomycin resistance cassette flanked by flp-recombinase recognition (FRT) sites, followed by the second *loxP* site. Downstream of the second *loxP* site was a splice acceptor site (SA)-stop-IRES-tdTomato cassette, followed by a WPRE (woodchuck hepatitis virus posttranscriptional regulatory element) to enhance mRNA stability, and an SV40 poly-A tail. The SA-stop cassette prevented the expression of the IRES-tdTomato until after cre-mediated recombination. The gene-targeting vector was then electroporated into R1 embryonic stem (ES) cells in the presence of neomycin. DNA from neomycin-resistant ES cells was then digested with BamHI, and Southern blotting was used to screen for homologous recombination. Chimeras were generated by injecting positive ES cell clones into C57/Bl6 mouse blastocysts. All experiments for generating the mice were performed at HHMI's Janelia Farm Research Campus under the direction of Dr. Caiying Guo. The neomycin resistance cassette was removed from the initially obtained mutant mice by crossing the KI mice to mice expressing flp-recombinase, and mice were then bred using standard procedures. All mice were maintained on a hybrid C57/Bl6 background.

Genotyping was performed by PCR using the following primers: Cbln2 forward: 5′-TAAAAGACAGTCCAGAGTTTTAGTC-′3, reverse: 5′-TGTGCTTACTCCTCTCTATTTGA-′3, and reverse: 5′-CTATTGGAGTCCTTCAAGGAAA-′3 (expected products, WT=225 bp, floxed=320 bp, and KO=420 bp). Cbln4 forward: 5′- CACAGATCTGTATTTCAAGGCA-′3, reverse: 5′-TGGATTTATTTCTTGGTGAGACATG-′3, and reverse: 5′-AGTCCTTCAAGGAAACAAACTT-′3 (expected products: WT=234 bp, floxed=315 bp, and KO=459 bp.

Quantitative RT-PCR

The following brain regions were dissected from male mice at post-natal day (P)0, P7, P14, P21, and P60: olfactory bulb, prefrontal cortex, hippocampus, striatum, thalamus, brainstem, cerebellum, and spinal cord. Total RNA was extracted using TRIzol according to the manufacturer's directions (Invitrogen). Samples were collected from 4 different mice; two experiments were done, and each experiment contained a biological duplicate and technical

triplicate. Samples were prepared for qRT-PCR using the VeriQuest Probe One-Step qRT-PCR Master Mix (Affymetrix) according to the manufacturer's instructions, and reactions was carried out and quantified using a 7900HT Fast RT-PCR instrument (Applied Biosystems). Transcript levels were normalized to the internal control β-actin. The following predesigned PrimeTime qPCR Assays were purchased from Integrated DNA Technologies (IDT): Cbln1 forward: 5′- GAGCCGTCCGAGATGAGTA-′3, reverse: 5′- CAACTTTGACTCAGAACGCAG-′3, and probe: 5′- TCGACCAGGTACTAGTGAACATCGGG-′3, Cbln2 forward: 5′- CGTACCATGACCATCTACTTCG-′3, reverse: 5′- TGTAGCACCAAGAAAGGGAAT-′3, and probe: 5′- AACCACTTTGACCTTGCCTCCAGT-′3, and Cbln4 forward: 5′- CAACCACGAGCCATCTGA-′3, reverse: 5′- CATTGGAATCTGTCTTTGTGGC-′3, and probe: 5′- AGCAACAAGACTCGCATCATTTACTTTGATC-′3.

Immunohistochemistry

For all immunohistochemistry, 3-week-old Cbln2-mVenus or Cbln4-mVenus mice were anesthetized with isoflurane and their brains were fixed by transcranial perfusion of 4% paraformaldehyde (PFA). Following removal from the skull, brains were further incubated in 4% PFA for 2 h at room temperature (RT) with agitation. Brains were then cryoprotected with 30% sucrose (in 1X PBS) at 4°C for 48 h with rotation. The samples were frozen in OCT compound (TissueTek) on dry ice, and 25 μm coronal or sagittal sections were produced with a cryostat (CM 3050S; Leica Biosystems). Sections were carefully transferred to a 1.5 mL tube and blocked with 10% goat serum, 1% BSA, 0.3% Triton X-100 in 1X PBS for 1 h at RT with rocking. Sections stained for GFP only were incubated in primary antibody overnight at 4°C with rocking; all other antibodies were incubated for 48 h at 4°C. Sections were washed 3 times for 20 min with PBS containing 0.3% Triton X-100, and incubated for 2 h at RT in species-specific secondary antibodies coupled to Alexa Fluor 488, 546, 633, or 647 (Invitrogen; 1:400 dilution). Sections were washed and mounted on slides with Vectashield containing the nuclear stain DAPI (Vector Laboratories).

All of the images in this study used GFP antibody to amplify the mVenus signal in the Cbln2-mVenus and Cbln4-mVenus mice. Heterozygous $Cbln2^{+/-}$-tdTomato; $Cbln4^{+/flox}$-mVenus mice were used to visualize co-expression of Cbln2 and Cbln4, and all of these sections were stained with anti-mCherry and anti-GFP. Because the mVenus in the $Cbln2^{flox/flox}$ sections was excited by both 488 nm and 546 nm lasers (see Figure 3a), only 633 nm or 647 nm excitable fluorescent dyes were used as secondary antibodies in all Cbln2 co-labeling experiments.

Whole sections were imaged using an Olympus VS110 scanning microscope with a 20× objective (Olympus Life Science Solutions). Higher resolution images for co-labeling experiments were collected using a Nikon A1R confocal (Nikon Instruments) with a 20× objective. Semi-automatic cell counting was done using ImageJ software. For each marker, at least two mice and four sections per brain region per mouse were used for detailed analyses, including semi-quantitative assessments. Expression patterns were confirmed in multiple additional mice in subsequent experiments that were not analyzed in detail.

Antibody characterization

The polyclonal mCherry antibody was raised in rabbit against recombinant full-length mCherry protein. mCherry is a derivative of red fluorescent protein (RFP) and antibodies raised against mCherry can detect mCherry and other RFP derivatives including tdTomato. mCherry was validated for use as a marker for tdTomato in both western blot and immunohistochemistry (see Figure 2). All other primary antibodies used are commercially available and have been previously validated (Table 1).

The monoclonal calbindin antibody was raised against bovine kidney calbindin-D, clone 6B-955. According to the manufacturer, this antibody does not react with other members of the EF-hand family, such as calbindin-D-9K, calretinin, myosin light chain, parvalbumin, S-100a, S-100b, S-100A2 (S100L), and S-100A6 (calcyclin). The monoclonal calretinin antibody was raised against recombinant rat calretinin, clone 6B8.2. The antibody is specific to brain and is routinely verified by the manufacturer by western blot on mouse brain lysates. The monoclonal CAMKII antibody was raised against partially purified rat CaM Kinase II, α-subunit, clone 6G9, and is routinely evaluated by the manufacturer by western blot. The polyclonal GFP antibody was raised against purified recombinant green fluorescent protein and was verified by the manufacturer by western blot and immunohistochemistry (IHC) using transgenic mice expressing GFP. We further verified the use of this antibody for detecting mVenus in both western blot and IHC (see Figure 2). The monoclonal parvalbumin antibody was raised against frog muscle parvalbumin, clone PARV-19. According to the manufacturer, this antibody recognizes parvalbumin in a Ca^{2+}-dependent manner, and does not react with other members of the EF-hand family. The polyclonal somatostatin antibody was raised against synthetic somatostatin coupled to keyhole limpet hemocyanin (KLH) with carbodiimide (CDI) linker. The specificity of the antibody was verified by the manufacturer by IHC; immunolabeling was abolished following pre-adsorption with somatostatin, somatostatin 25, and somatostatin 28. The monoclonal tyrosine hydroxylase (TH) antibody was against TH purified from PC12 cells, clone LNC1. This antibody is routinely evaluated by the manufacturer by western blot on mouse brain lysates.

Statistics

qRT-PCR data were analyzed by one-way Kruskal-Wallis analysis of variance (ANOVA) using GraphPad Prism 6. Graphs depict mean ± S.E.M. and asterisks denote statistical significance where $*p \leq 0.05$, $**p \leq 0.01$, $***p \leq 0.001$, $****p \leq 0.0001$.

RESULTS

Expression of Cbln1, Cbln2, and Cbln4 throughout brain during development

Because mutations in Cbln1 produce a prominent cerebellar phenotype, much is known about its expression and function in cerebellum (Hirai et al., 2005; Iito-Ishida et al., 2008). Moreover, recent studies have suggested a role for Cbln1 in other brain regions (Kusnoor et al., 2010; Otsuka et al., 2016). Cbln2 and Cbln4, however, are poorly understood (note that Cbln3 only functions in conjunction with one of the other three cerebellins; Pang et al., 2000; Bao et al., 2006), and even for Cbln1, few systematic, quantitative analyses are

available. Thus, we first assessed the relative expression of cerebellins in brain during development. We measured the mRNA levels of Cbln1, Cbln2, and Cbln4 in different brain regions and at different developmental stages by quantitative reverse-transcription PCR (qRT-PCR), using the housekeeping gene β-actin as an internal standard.

In examining the absolute levels of Cbln1, Cbln2, and Cbln4 mRNAs in newborn mice at P0, we found that Cbln1 and Cbln2 are abundantly expressed throughout brain, with generally higher levels in the cortex and olfactory bulb than in the hippocampus, striatum, and thalamus (Figure 1a). In most brain regions, Cbln2 was more abundant than Cbln1; in the prefrontal cortex, Cbln2 levels reached an astounding ~13% of levels of β-actin, a very abundant transcript! Cbln4, by contrast, was present at much lower levels in all brain areas (<0.5% of β-actin; Figure 1a).

At birth, Cbln2 levels in the mouse cerebellum were ~10% of those of β-actin, and nearly 5-fold higher than those of Cbln1. However, cerebellar Cbln2 levels decreased ~100-fold during postnatal development to <0.1% of β-actin levels in adults (Figure 1b). In contrast, cerebellar Cbln1 levels increased dramatically during postnatal development (~20-fold). As a result, Cbln1 expression rose to extraordinarily high levels in adult cerebellum, reaching ~40% of β-actin levels and explaining its naming for the cerebellum (Urade et al., 1991). Thus, Cbln1 and Cbln2 expression switches during development, and overall cerebellin levels do not decrease in cerebellum after synaptogenesis, but remain very high even in adult mice at P60 (Figure 1b). These results confirm a previous study showing a similar developmentally regulated swap between Cbln1 and Cbln2 (Rong et al., 2012). Cbln4 mRNA in the cerebellum was detected at very low levels (~0.002% of β-actin) or could not be detected at all, and was therefore not included in this analysis.

We next monitored the developmental expression profile of individual cerebellins in different brain regions of mice by measuring Cbln1, Cbln2, and Cbln4 mRNA levels at different ages. We observed strikingly different developmental dynamics of cerebellin expression in different brain regions. Some regions exhibited no developmental change in the expression of a cerebellin (for example, all cerebellins in olfactory bulb and spinal cord; Cbln2 in prefrontal cortex; Figure 1c), while others displayed large monotonic increases (for example, Cbln4 in prefrontal cortex [~40-fold] and brainstem [~3-fold], Figure 1c), or large decreases (for example, Cbln1 in prefrontal cortex and hippocampus [both ~3-fold], Figure 1c), or initial increases followed by decreases (for example, Cbln1 in thalamus, Cbln2 in striatum, Figure 1c). Thus, no canonical developmental time course guides cerebellin expression, and cerebellin function is not restricted to a particular developmental period, such as synaptogenesis.

Design of Cbln2 and Cbln4 reporter mice

In order to further characterize the expression and function of cerebellins, we generated a new genetic tools for Cbln2 and Cbln4 that complement those available for Cbln1 (Figure 2a). We used homologous recombination in embryonic stem cells to produce mutant mice in which the endogenous Cbln2 or the Cbln4 gene expressed a fluorescent reporter gene for monitoring gene expression, and were simultaneously rendered sensitive to Cre-recombinase, i.e. became conditional knockout alleles. For this purpose, we introduced loxP

sites into the first intron 5′ of exon 2, inserted an internal ribosome entry site (IRES) sequence followed by an mVenus coding sequence into the part of exon 3 that encodes the 3′ untranslated region of the Cbln2 or Cbln4 mRNA, and introduced a second loxP site 3′ to the mVenus sequence. Furthermore, we added an artificial exon with a splice-acceptor site, a stop codon, and an IRES sequence followed by the tdTomato coding sequence into the intron 3′ to exon 3 (Figure 2a). According to this design, the knockin alleles will co-express mVenus with Cbln2 or Cbln4 prior to cre-mediated recombination. Cre-mediated recombination will delete mVenus and exons 2 and 3 of Cbln2 or Cbln4 coding sequences, and cause the remaining exon 1 to splice into the artificial Stop-IRES-tdTomato exon. Therefore, these mice were constructed to serve both as a tool to monitor Cbln2 or Cbln4 expression, and to allow conditional or constitutive deletion of Cbln2 or Cbln4. Mice carrying the wildtype, floxed, and/or KO Cbln2 and Cbln4 alleles were genotyped by PCR (Figure 2b).

To validate the targeting strategy, we analyzed by immunoblotting brain homogenates from control mice, from heterozygous floxed knockin or cre-recombined KO mice ($Cbln2^{+/F}$ or $Cbln4^{+/F}$, or $Cbln2^{+/-}$ or $Cbln4^{+/-}$, respectively), and from compound floxed/KO mice ($Cbln2^{F/-}$ or $Cbln4^{F/-}$). We monitored expression of mVenus using antibodies to GFP (which recognize mVenus), and of tdTomato using antibodies to mCherry (which is duplicated in tdTomato). We observed robust mVenus expression exclusively in mice with floxed alleles as expected. However, we detected only weak expression of tdTomato in mice with KO alleles (Figure 2c), possibly because the deletion of most of the Cbln2 or Cbln4 coding region will result in an mRNA that is subject to non-sense-mediate decay and thus produces very little tdTomato synthesis.

To further validate the knockin mice, we imaged mVenus or tdTomato expression in coronal sections from knockin and KO mice, using detection of mVenus or tdTomato via their intrinsic fluorescence or by immunohistochemistry. We examined the sections on a confocal microscope with excitation at 488 nm or 546 nm to selectively excite mVenus or tdTomato, respectively, or the secondary fluorescently labeled-antibodies used for immunohistochemistry of these proteins.

Sections from Cbln2 knockin mice exhibited bright mVenus fluorescence; mVenus was identically detected by immunohistochemistry (Figure 3a). The mVenus signal, with or without antibody staining, was abolished by KO of Cbln2, confirming the design of the genetic manipulation (Figure 3b). In Cbln4 knockin mice, mVenus fluorescence was much weaker than in Cbln2 knockin mice (Figure 3c) and required the use of antibodies to be detected, presumably because of the much lower expression levels of Cbln4 (Figure 1). Nevertheless, enhanced Cbln4-mVenus detection by immunohistochemistry allowed mapping of Cbln4 expression (Figure 3c). Cbln4-mVenus fluorescence and immunohistochemical detection were also abolished upon KO of Cbln4 as expected (Figure 3d).

When we analyzed tdTomato fluorescence in Cbln2 knockin and Cbln2 KO mice, we observed a specific but weak signal in both. Because there was no tdTomato band in the floxed sample in the immunoblot (Figure 2c), the tdTomato signal in the Cbln2 knockin

mice was likely due to partial excitation of mVenus by 546 nm light (Figure 3a,b). In Cbln4 knockin mice, we detected no tdTomato fluorescence signal, but again observed a weak signal in the Cbln4 KO mice following enhanced detection by immunohistochemistry (Figure 3c,d). In all instances, the spatial distributions of mVenus and tdTomato expression were indistinguishable.

Viewed together, these results suggest that the Cbln2 and Cbln4 reporter mice reliably reveal Cbln2 and Cbln4 expression with a distinct spatial distribution, and additionally allow monitoring Cbln2 or Cbln4 deletions. Thus, the strategy involving IRES-mediated expression of mVenus in knockin mice worked well, although IRES-tdTomato expression was much weaker in KO mice, possibly due to nonsense-mediated decay of the mRNAs containing the deleted Cbln2 or Cbln4 coding sequences.

Overall Cbln2 and Cbln4 expression patterns

Using the mVenus signal, we surveyed the overall expression of Cbln2 and Clbn4 in adult mouse brain (Figure 4). We observed robust Cbln2 expression throughout the brain, with the highest levels in the olfactory bulb, cortical structures, and the thalamus (blue in Figure 4). Compared to Cbln2, Cbln4 expression was weak, but was clearly detectable by immunohistochemistry in distinct regions throughout the brain, with the highest levels in the retrosplenial cortex, entorhinal cortex, and the zonal layer of the superior colliculus (green in Figure 4). Because the expression of Cbln2 was so much greater than Cbln4, when assessing the intensity of expression we only compared the relative expression of each gene to itself. For example, Cbln4 is highly expressed in the entorhinal cortex compared to the expression of Cbln4 in other brain regions, but the absolute level of Cbln4 expression is much lower based on the mRNA measurements shown in Fig. 1. Overall, Cbln4 is more widely expressed, but Cbln2 is more highly expressed.

In the following, we will analyze selected brain regions in greater detail to illustrate several general principles that emerged from the localizations of Cbln2 and Cbln4. Specifically, we found that the expression of Cbln2 and Cbln4 is highly heterogeneous and not uniformly observed in neurons; we also found that Cbln2 or Cbln4 are mostly expressed in distinct, non-overlapping populations of neurons; and finally, we observed that they are mostly, but not exclusively, expressed by projection neurons.

Cbln2 and Cbln4 are expressed in multiple olfactory nuclei

In the main olfactory bulb (MOB), Cbln2 was robustly expressed in two classes of inhibitory interneurons: periglomerular cells (PGCs) and granule cells (Figure 5a–d). PGCs can be subdivided into three non-overlapping populations based on the presence of calbindin (CB), calretinin (CR), and tyrosine hydroxylase (TH; Kosaka et al., 1995). Co-labeling experiments revealed that 60% of $Cbln2^+$ PGCs were also CB^+ (n=1594; Figure 5c), but only 4% were CR^+ (n=1543; Figure 5d). $Cbln2^+$ PGCs never co-localized with TH. Thus, Cbln2 expression further subdivides CB^+-PGCs into two classes.

In contrast to Cbln2, Cbln4 was primarily expressed in the MOB by excitatory mitral neurons (Figure 5e–g). These neurons receive inhibitory inputs from both PGCs and granule cells, and are the output neurons of the MOB (Orona et al., 1984). $Cbln4^+$ axons can be seen

exiting the MOB and traveling down the lateral olfactory tract before terminating in the medial nuclei of the amygdala (Figure 5g). Double-labeling of heterozygous Cbln2$^{+/-}$-tdTomato/Cbln4$^{+/flox}$-mVenus sections of the MOB revealed intermingling between the dendrites of Cbln2^{+} PGCs and of Cbln4^{+} mitral cells (Figure 5f *bottom*), presumably forming dendrodendritic synaptic connections.

In the accessory olfactory bulb (AOB), Cbln2 expression was observed in both excitatory mitral cells and inhibitory PGCs (Figure 5a), whereas Cbln4 expression again was only observed in mitral cells (Figure 5e). In double labeling experiments, 85% of mitral cells in the AOB expressed both Cbln2 and Cbln4; of the remaining cells, 9% expressed only Cbln2 and 6% expressed only Cbln4 (n=961; Table 3).

In olfactory cortical regions, Cbln2^{+} neurons were observed throughout the endopiriform cortex (Den), which lacks a layered structure, and in layer 2 of the three layers of the piriform cortex (Pir; Figure 5h). The three layers of the piriform cortex consist of a superficial molecular layer (layer 1), a densely packed pyramidal layer (layer 2), and a deep polymorphic layer (layer 3) (Neville and Haberly, 2004). Layer 2 neurons are primarily excitatory pyramidal cells, with a small population of inhibitory stellate and bipolar cells. Layer 2 neurons receive excitatory afferents from MOB via the lateral olfactory tract, and send excitatory efferents to other cortical regions (Kay and Freeman, 1998; Neville and Haberly, 2004). Consistent with these findings, no Cbln2^{+} neurons in piriform cortex were co-labeled with CB or PV, and only a few sparse Cbln2^{+} neurons showed CR immunoreactivity (Table 2). These results, combined with cell morphology assessments, show that most Cbln2^{+} neurons in the piriform cortex are excitatory pyramidal cells. No significant Cbln4 expression was observed in these cortical regions (Figure 5g).

Olfactory regions send projections to the amygdaloid complex (Sah et al., 2003). Cbln2 expression was largely absent from the amygdala, and was only observed in the nucleus of the lateral olfactory tract (NLOT; Figure 5h). The NLOT has a distinctive layered structure consisting of an inner polymorphic layer (III), a middle pyramidal layer (II) and an outer molecular layer (I) containing fibers from layer II, as well as axons from the MOB and AOB (Santiago and Shammah-Lagnado, 2004). Densely packed Cbln2^{+} somata were found in layer II, and Cbln2^{+} fibers were seen in layer I, where they joined the lateral olfactory tract. All Cbln2^{+} neurons in the NLOT co-localized with CAMKII, confirming that these neurons are excitatory.

In contrast to Cbln2, Cbln4 was detected in a small subset of neurons in multiple nuclei throughout the amygdala. The nuclei of the amygdaloid complex are divided into a superficial cortical-like, a basolateral, and a centromedial group. In the superficial cortical-like group, Cbln4^{+} neurons were seen in the amygdalo-hippocampal area (AHA), anterior cortical nucleus (CoAa), and peri-amygdaloid complex (PAC), but were notably absent from the NLOT (Figure 5g,i). The peri-amygdaloid complex has a layered structure similar to the NLOT, and Cbln4^{+} somas were similarly found in the pyramidal cell layer II. Cbln4^{+} neurons in this region were pyramidal-like cells with a large, spiny apical dendrite that extends vertically and perpendicular to the surface of the brain, similar to pyramidal neurons

in the cerebral cortex, in addition to many basal dendrites that project in all directions (Figure 5i).

Neurons of the basolateral group are cortical-like, with ~ 70% excitatory pyramidal-like and ~30% inhibitory stellate-like cells. The latter can be subclassified based on the expression of CB, CR, and PV (McDonald, 1998; McDonald and Mascagni, 2001). Densely packed Cbln4$^+$ somas were found in the anterior basolateral nucleus (BLA) and the dorsolateral and ventromedial subdivisions of the lateral nucleus (LAdl, and LAvm). A few scattered neurons were seen in the posterior basolateral (BLP), basal medial (BM), and ventrolateral LA (LAvl; Figure 5i). Cbln4$^+$ neurons strongly co-localized with CAMKII (Figure 5j), and did not co-localize with CB, CR, or PV (Table 2), suggesting that all of the Cbln4$^+$ neurons in the BLA group are excitatory.

Neurons in the centromedial group largely resemble inhibitory striatal medium-spiny neurons (Alheid and Heimer, 1988; Sah et al., 2003). Within this group, Cbln4 was expressed in the anterior amygdaloid area (AA), the anterolateral (AL) and anteromedial (AM) subdivisions of the BNST, the medial subdivision of IPAC, the infra-amygdaloid subdivision of the bed nucleus of the stria terminalis (BSTia), the amygdostriatal transition area (AStr), and the dorsal subdivision of the medial nucleus (MEd; Figure 5i). Cbln4$^+$ neurons in most of these nuclei did not co-localize with the inhibitory markers CB, CR, or PV, except in the MEd where a small subset of Cbln4$^+$ neurons co-localized with CR (Figure 5k; Table 2).

Cbln2 and Cbln4 are expressed throughout the cortex

Strong Cbln2 expression was observed in layers 2/3, 5 and 6a of most areas of the cerebral cortex, while Cbln4 expression was mostly limited to layer 2/3 and, to a lesser degree, layer 5 (Figure 6a,f).

Excitatory pyramidal and stellate neurons account for ~80% of cortical neurons (Potter et al., 2009); the remaining ~20% inhibitory neurons can be classified into three overall groups based on their expression of CB, CR, or PV (Kubota et al., 1994; Molyneaux et al., 2007; Potter et al., 2009). Most Cbln2$^+$ neurons in the cortex were small to medium-sized pyramidal cells in layer 2/3 and large pyramidal cells in layer 5 (Figure 6b,c). Dense Cbln2$^+$ fibers projected into the dorsal striatum from the layer 5 neurons (Figure 6a *white arrows*). Cbln2 expression was also detected in vertically oriented bipolar cells, aspiny multipolar cells, and double bouquet cells (Figure 6c). Cbln2$^+$ somata were seen in all 6 cortical layers, although only sparse expression was observed in layers 1 and 4.

In co-labeling experiments, 70% (n=1,386) of Cbln2$^+$ neurons in layer 2/3 SS cortex co-expressed CB (Figure 6d), which is characteristic of both inhibitory neurons in layers 2-6, and pyramidal neurons in layer 2/3 (Hayes and Lewis, 1992). Previous studies have shown that CB antibodies brightly stain the somata, axons and dendrites of inhibitory neurons, but only weakly the somata of pyramidal neurons, and do not stain their axons or dendrites (DeFelipe and Fariñas, 1992; Kubota et al., 1994; Hayes and Lewis, 1995; Hof et al., 1998). None of the bright CB$^+$ neurons in layer 2/3 expressed Cbln2, and none of the apparently inhibitory Cbln2$^+$ neurons (based on morphology) showed CB immunoreactivity (Figure

6d). Additionally, Cbln2$^+$ neurons in layer 5 did not co-express CB, and only a few scattered co-labeled neurons were observed in layer 4 or 6 (Table 2). Taken together, these data show that all of the Cbln2$^+$/CB$^+$ double positive neurons in layer 2/3 are excitatory, and that the Cbln2$^+$ inhibitory neurons in the cortex lack CB. Conversely, although only 4% of Cbln2$^+$ layer 2/3 neurons expressed CR, ~60% of CR-positive (CR$^+$) neurons in layer 2/3 co-localized with Cbln2 (n=1,545; Figure 6e). A few scattered Cbln2$^+$/CR$^+$ co-labeled neurons were found in layers 4-6, but these cells accounted for <1% of Cbln2$^+$ neurons in these layers. Overall, these results suggest that ~96% of all Cbln2$^+$ neurons in the cortex are excitatory, and only ~4% are inhibitory (Table 2).

Based on morphology and co-labeling, the majority of Cbln4$^+$ neurons observed in layer 2/3 were also excitatory pyramidal cells; ~45% of these Cbln4$^+$ neurons co-expressed CB. Cbln4 expression was additionally observed in stellate cells, double bouquet cells, chandelier cells, and layer 5 pyramidal neurons (Figure 6g,h). Different from what we observed for Cbln2, 10% of Cbln4$^+$ layer 2/3 neurons appeared to be brightly-labeled CB$^+$ inhibitory neurons, and only 35% of Cbln4$^+$ layer 2/3 neurons were CB$^+$ excitatory neurons (n=1,386; Figure 5i). Additionally, 5% of Cbln4$^+$ neurons in layer 2/3 co-expressed CR (n=993; Figure 6j). These results show that ~85% of Cbln4$^+$ neurons in the cortex are excitatory and ~15% inhibitory. No Cbln2 or Cbln4 expression was observed in PV$^+$ neurons anywhere in the cortex (Table 2).

Double labeling of heterozygous Cbln2$^{+/-}$-tdTomato; Cbln4$^{+/flox}$-mVenus sections (in which the tdTomato signal reports on Cbln2 expression, and the mVenus signal on Cbln4 expression) revealed that 20% of labeled neurons in layer 2/3 expressed both Cbln2 and Cbln4, while 45% expressed only Cbln2, and 35% only Cbln4 (n = 2,410). Similarly, in layer 5, 20% of labeled neurons expressed both Cbln2 and Cbln4, 55% expressed only Cbln2, and 25% expressed only Cbln4 (n = 2,881; Table 3). Thus, despite their overall similar expression patterns, Cbln2 and Cbln4 are mostly expressed in distinct neuronal populations in the cortex.

Retrosplenial cortex and hippocampal formation

Recent experiments have identified a network of highly interconnected brain regions that are involved in spatial memory and cognition, and that include the retrosplenial cortex, the hippocampal formation including the entorhinal cortex, and the anterior nuclei of the thalamus (Wyss and van Groen, 1992; Sugar et al., 2011; Miller et al., 2014). Cbln2 and Cbln4 again exhibit interesting expression patterns in these regions.

The retrosplenial cortex (RSC), located along the midline posterior to the cingulate cortex, is subdivided into granular (Rg) and dysgranular (Rdg) sections. The layered structure of the retrosplenial cortex resembles that of other cortical regions, except that Rgd lacks a well-defined granular layer 4 (van Groen and Wyss, 1990; Wyss and van Groen, 1992). Similar to other cortical regions, Cbln2$^+$ neurons were found in layers 2/3 and 5 of the Rdg and Rg sections of the retrosplenial cortex (Figure 7a). However, different from other cortical regions where Cbln2 is uniformly expressed in layer 2/3 neurons, Cbln2$^+$ neurons were only observed in a scattered pattern in the upper layer 2 but otherwise absent from layer 2/3 (Figure 7b). Cbln4, conversely, was expressed in densely packed pyramidal cells in layer 2/3

of Rdg, but not in Rg (Figure 7c). These Cbln4$^+$ neurons were distinguished by the presence of a highly branched, short apical dendrite, and a long, vertically oriented axon that could be seen traveling the length of the cortex and entering the corpus callosum (Figure 7d). These layer 2/3 projection neurons in the Rdg send projections to the contralateral orbitofrontal cortex, anterior cingulate cortex, subiculum, entorhinal cortex, subcortical regions, and the retrosplenial cortex (Wyss and van Groen, 1992; Sugar et al., 2011; Miller et al., 2014). Consistent with these findings, Cbln4$^+$ neuropil was also observed in layer 5 of the Rdg (Figure 7d *arrow heads*), potentially arising from Cbln4$^+$ neurons in the contralateral Rdg. In co-labeling experiments, <10% of Cbln4$^+$ neurons in layer 2/3 Rdg co-expressed CB, and none of these neurons co-expressed Cbln2 (Table 2).

The hippocampal formation consists of the hippocampus proper (CA1, CA2, and CA3 regions), dentate gyrus, subiculum, and entorhinal cortex (ENT; Sugar et al., 2011). In the hippocampal formation, the strongest Cbln2 expression was observed in the pyramidal cells of the subiculum (Figure 7e,g). The excitatory pyramidal neurons of the subiculum project via the fornix to various cortical and subcortical targets, including the retrosplenial and entorhinal cortices and the anterior nuclei of the thalamus (van Groen and Wyss, 1990; Dolorfo and Amaral, 1998; Sugar et al., 2011; Miller et al., 2014). Consistent with these known projections, robustly Cbln2-positive neuropil was observed in the anteroventral (AV) and lateral dorsal (LD) thalamic nuclei (Figure 8a,b). Little Cbln2 expression was detected in the hippocampal formation outside of the subiculum, with only sparse Cbln2$^+$ neurons observed in the CA1-CA3 regions and the dentate gyrus (Figure 7e). None of these Cbln2$^+$ neurons co-expressed parvalbumin (PV), and a few scattered cells co-expressed CB or CR (Table 2).

Cbln4 was most highly expressed in the hippocampal formation in layer 2 and layer 3 of the medial (ENTm) and lateral (ENTl) entorhinal cortex and the ventral subiculum (Figure 7c). Layer 2 of ENT contains two major cell types, CB$^+$ excitatory pyramidal and CB$^-$ stellate neurons (Alonso and Klink, 1993; Naumann et al., 2015), whereas layer 3 primarily contains excitatory pyramidal neurons (Chrobak et al., 2000). Nearly all Cbln4$^+$ neurons in layer 2 were CB$^+$ (Table 2), suggesting that most of the Cbln4$^+$ neurons in the entorhinal cortex are excitatory pyramidal cells. Layer 2 neurons send projections to the molecular layer of dentate gyrus and the S. moleculare-lacunosum of the CA3 region, whereas layer 3 neurons send projections to the S. moleculare-lacunosum of the CA1 region (Chrobak et al., 2000). Consistent with these projection patterns, dense Cbln4$^+$ fiber bundles from the ENT were observed in the molecular layer of CA1, CA3, and dentate gyrus (Figure 7c,f,h).

In the ventral subiculum, co-labeling of heterozygous Cbln2$^{+/-}$-tdTomato/Cbln4$^{+/flox}$-mVenus sections confirmed that Cbln2 and Cbln4 were largely expressed in non-overlapping layers, although a few neurons in the stratum radiatum contained both (Figure 7i). Similar to Cbln2, Cbln4 was expressed only sparsely and at low levels in neurons of CA1 and CA3 regions and the dentate gyrus (Figure 7f). Unlike Cbln2, parvalbumin immunoreactivity was observed in ~50% of Cbln4$^+$ neurons in CA1, ~60% of Cbln4$^+$ neurons in CA3, and ~43% of Cbln4$^+$ neurons in the dentate gyrus. Similar to Cbln2, only a few scattered Cbln4$^+$ neurons in the hippocampus co-expressed calbindin or calretinin (Table 2).

Differential Cbln2 and Cbln4 expression in the thalamus

Cbln2 or Cbln4 expression was not detected in the anterior group of thalamic nuclei (the anteromedial (AM), anterodorsal (AD), anteroventral (AV), and lateral dorsal (LD) nuclei), although $Cbln2^+$ neuropil was observed in the ventrolateral subdivision of the anteroventral (AVVL) and in LD (Figure 8a,b). In the ventral group of thalamic nuclei (comprising the ventroanterior (VA), ventrolateral (VL), ventromedial (VM), ventral posteromedial (VPM), and ventral posterolateral (VPL) nuclei), Cbln2 was highly expressed in the VA and VL nuclei (Figure 8b), which are the motor nuclei of the thalamus that receive major inputs from the basal ganglia and cerebellum (Sommer, 2003). All $Cbln2^+$ neurons in the VL co-expressed CB, which is present in a subset of VL neurons (Figure 8f). Cbln4 immunoreactivity was absent from the ventral nuclear group (Figure 8j).

In the midline group of thalamic nuclei, modest Cbln2 expression was observed in neurons of the paraventricular (PVT), intermediodorsal (IMD), and reuniens (N.re) nuclei (Figure 8a,b). 61% of $Cbln2^+$ neurons in PVT were CB^+ (n=462; Figure 8d), and 90% were CR^+ (n=351; Figure 8e). In the N. Re, 68% of $Cbln2^+$ neurons were CB^+ (n=314) and 78% were CR^+ (n=898; Table 2). $Cbln4^+$ cell bodies as well as dense Cbln4-fiber bundles were also observed in PVT, IMD, and N.Re (Figure 8i,j). CB immunoreactivity was observed in 38% of $Cbln4^+$ neurons in PVT (n=1,275; Figure 8l), and 53% of $Cbln4^+$ neurons in N.Re (n=1,045; Table 2). Cbln4 expression highly co-localized with CR expression throughout the midline and intralaminar nuclear groups. Within the midline nuclei, CR immunoreactivity was observed in 93% of all $Cbln4^+$ neurons in PVT (n=842; Figure 8m), and 86% of $Cbln4^+$ neurons in N.Re (n=1,152; Table 2). In $Cbln2^{+/-}$-tdTomato; $Cbln4^{+/flox}$-mVenus sections, Cbln2 and Cbln4 were co-expressed in 33% of labeled PVT neurons (Figure 8p); of the remaining neurons, 11% expressed only Cbln2 and 57% expressed only Cbln4 (n=951). Similarly, 32% of labeled N.Re neurons expressed both Cbln2 and Cbln4, while 12% expressed only Cbln2 and 57% expressed only Cbln4 (n=1,135; Table 3).

In the intralaminar group of thalamic nuclei, dense Cbln2 expression was observed in the paracentral oval (POC) and parafasicular (PF) nuclei. Moreover, a few weakly $Cbln2^+$ neurons were observed in the central medial (CM) and rhomboid nuclei (Rh)(Figure 8b,s).

$Cbln4^+$ cell bodies, as well as dense fiber bundles were observed in CM, PCN, CL, and Rh (Figure 8j). In PF, Cbln4 appeared to be expressed in every neuron (Figure 8s), and $Cbln4^+$ fibers from these neurons could be seen traveling to the striatum (Figure 8j *arrows*). In double labeling of heterozygous $Cbln2^{+/-}$-tdTomato; $Cbln4^{+/F}$-mVenus sections, all of the labeled neurons in PF expressed both Cbln2 and Cbln4 (Figure 8s). Consistent with previous reports (Jones and Hendry, 1989; Frassoni et al., 1991; Jacobowitz and Winsky, 1991), no CB^+, CR^+ or PV^+ cell bodies were observed in PF. A few scattered CB+ neurons were found in OPC, but they did not co-localize with Cbln2+ neurons (Table 2).

Neither Cbln2 nor Cbln4 expression was seen in the reticular nucleus or the medial nuclear group of the thalamus (Figure 8a–b, i–j).

The medial geniculate body of the thalamus consists of ventral, dorsal, and medial subdivisions (MGBv, MGBd, and MGMm, respectively). The paralaminar nuclear group

comprises the supragenicular (SG), posterior intralaminar nucleus (PIN), and the peripeduncular nucleus (PP). Together these nuclei form the MGB/paralaminar complex, and relay auditory information between the inferior colliculus and auditory cortex. The neurons in MGBv are PV^+ but lack CB or CR, whereas the neurons in the MGBd, MGBm, and paralaminar nuclei are all devoid of PV and differentially express CB and/or CR (Lu et al., 2009).

Both $Cbln2^+$ (Figure 8c) and $Cbln4^+$ (Figure 8k) somata were observed throughout the medial geniculate body and the paralaminar nuclei group of the thalamus with the exception of the ventral subdivision of the medial geniculate body (MGBv). Overall, 58% of $Cbln2^+$ neurons were CB^+ (n=2,300; Figure 8g), and 70% were CR^+ (n=2,014; Figure 8h), while 37% of $Cbln4^+$ neurons were CB^+ (n=934; Figure 8n), and 45% were CR^+ (n=1,422; Figure 8o). Double labeling of $Cbln2^{+/-}$-tdTomato; $Cbln4^{+/F}$-mVenus sections revealed that 42% of labeled neurons in the medial geniculate body/paralaminar complex expressed only Cbln4, 34% expressed only Cbln2, and 24% expressed both Cbln4 and Cbln2 (n=1,673; Figure 8q; Table 3).

In the lateral geniculate nucleus, Cbln2 and Cbln4 were both expressed in the intergeniculate leaflet (IGL) and the ventral subnucleus (VGN), but not in the dorsal subnucleus (DLG) (Figure 8r). Double labeling of heterozygous $Cbln2^{+/-}$-tdTomato; $Cbln4^{+/F}$-mVenus sections revealed that Cbln2 and Cbln4 were co-expressed in 35% of labeled IGL neurons (n=312). The VGN contains multiple subdivisions, the lateral (VLGl), intermediate (VLGi), and medial subdivisions (VLGm; Chrobok et al., 2016). 54% of VLGi neurons (n=333), and 15% of VLGl neurons (n=185; Figure 8r *right*) co-expressed Cbln2 and Cbln4. Of the remaining neurons, 48% of IGL neurons, 19% of VLGi neurons, and 0% of VLGl neurons expressed only Cbln4 (Figure 8r *left*); whereas 17% of IGL neurons, 28% of VLGi neurons, and 85% of VLGl neurons expressed only Cbln2 (Figure 8r *middle*). Only sparse $Cbln2^+$ or $Cbln4^+$ neurons were found in VLGm (Table 2).

Expression of Cbln2 and Cbln4 in the hypothalamus

Within the hypothalamus, $Cbln2^+$ neurons were found in the ventrolateral subdivision of the suprachiasmatic nucleus (SChVL), the peri- and paraventricular hypothalamic nuclei (PVi and PVH, respectively), the dorsomedial nucleus (DMH), and the lateral hypothalamic area (LHA). Sparse $Cbln2^+$ neurons were also present in the medial preoptic area (MPA; Figure 9a–b). In PVH, 25% of $Cbln2^+$ neurons (n=761) co-expressed TH (Figure 9c). Partial overlap between Cbln2 and CB or CR was observed in DMH (Figure 9d–e), PVi, and LHA (Table 2). High Cbln4 expression was seen in the medial preoptic nucleus (MPO), the arcuate nucleus (ARH), and the posterior hypothalamic area (PH), and moderate expression was seen in PVi, MPA, and DMH (Figure 9f–h). In PH, most of the $Cbln4^+$ neurons co-labeled with CB (Figure 9i) or CR (Figure 9j). Partial overlap between $Cbln4^+$ neurons and CB^+ or CR^+ neurons was observed throughout the hypothalamus, with the exception of ARH where $Cbln4^+$ neurons did not express CB or CR (Table 2).

Expression of Cbln2 and Cbln4 in the superior colliculus

The superior colliculus (SC) is organized into 6 layers: layers 1-3 are referred to as the superficial layers, and are involved in visual processing, whereas layers 4-6 are known as the deep layers, and are involved in visual, auditory, somatosensory, and motor processing (Huerta and Harting, 1984).

Cbln2 was very highly expressed in neurons found in layer 3, the optic layer (Op; Figure 9k), and nearly all of these Cbln2$^+$ neurons co-expressed CB (Table 2). Previous studies have shown that the CB$^+$ neurons in optic layer are intrinsically bursting excitatory cells that receive direct inputs from the retina, and send projections to the lateral posterior nucleus of the thalamus (Huerta and Harting, 1984; Lo et al., 1998). Cbln4 expression was largely found in inhibitory horizontal neurons in layer 1, the zonal layer (Zo; Figure 9o). These Cbln4$^+$ neurons did not co-localize with CB, CR, or PV, and there was no overlap between Cbln2$^+$ and Cbln4$^+$ neurons throughout the superior colliculus (Table 2).

Expression of Cbln2 and Cbln4 in multiple nuclei of the auditory pathway

In addition to the aforementioned MGB/paralaminar complex, Cbln2 and Cbln4 expression was found in non-overlapping but complimentary nuclei within the classical auditory pathway. Cbln2$^+$ somas were observed throughout the superior olivary complex (SOC) and inferior colliculus (IC), and intense Cbln2 expression was observed in somas and neuropil of the dorsal nucleus of the lateral lemniscus (NLLd; Figure 9l). Cbln2 expression in the SOC was relatively weak compared to other Cbln2$^+$ nuclei, and could only be observed after antibody staining. The highest density of Cbln2$^+$ neurons was observed in the medial nucleus of the trapezoid body (MNTB; Figure 9l); all of the Cbln2$^+$ neurons in MNTB co-expressed CB (Figure 9m) and PV (Figure 9n). All of the Cbln2$^+$ somas in the other subdivisions of the SOC were also PV$^+$; no CB$^+$ or CR$^+$ cell bodies were observed outside of MNTB, consistent with previous studies that found the same pattern of PV, CB, and CR expression in SOC (Friauf, 1994; Lohmann and Friauf, 1996).

The inferior colliculus (IC) is separated into three subdivisions: a three-layered external cortical division (ECIC), a central division (CIC), and a dorsal cortical subdivision (DCIC; Ito et al., 2011). Robust Cbln2 expression was observed throughout the IC, with the notable exception of layer 3 of ECIC, where only sparse labeling was seen (Figure 9p). All of the Cbln2$^+$ neurons in IC are excitatory, based on co-expression with CAMKII (Table 2).

Cbln4 expression was largely restricted to the ventral cochlear nucleus (VCN), although sparse Cbln4$^+$ neurons were observed along the outer shell of ECIC (Figure 9p). The VCN is special in that it is the only nucleus in the auditory brainstem pathway where CR and PV are both expressed in the same neurons (Lohmann and Friauf, 1996). Consistent with this, 75% of Cbln4$^+$ cell bodies in the VCN co-labeled with CR (n=230; Figure 9q), and all of the Cbln4$^+$ cell bodies co-labeled with PV (Figure 9r). This suggests that a significant number of VCN neurons express all three. CB is also weakly expressed in the VCN (Friauf, 1994; Lohmann and Friauf, 1996), however no co-labeling of Cbln4$^+$ and CB$^+$ neurons was observed (Table 2).

DISCUSSION

Classical studies in cerebellum established that Cbln1 is of central importance for the function of parallel fiber synapses (Hirai et al., 2005; Ito-Ishida et al., 2008; Uemura et al., 2010). Motivated by these studies and the findings that Cbln1 belongs to a family of conserved neurexin-binding proteins that are broadly expressed in brain (Miura et al., 2006; Wei et al., 2012), we here investigated the relative distributions of the other two autonomously functioning cerebellin isoforms, Cbln2 and Cbln4. For these investigations, we generated new genetic tools that allow monitoring expression of Cbln2 and Cbln4 (Figure 2). Our data demonstrate that Cbln2 and Cbln4 are expressed in specific, largely non-overlapping and well-defined subsets of neurons throughout the brain. Our results suggest that cerebellins are broadly functioning genes with diverse expression patterns and distinct roles; most importantly, high-level expression of Cbln2 and Cbln4 (and probably Cbln1) is restricted to small subpopulations of neurons throughout the brain, suggesting specialized neuron-specific functions.

As measured by quantitative RT-PCR, cerebellins were expressed overall abundantly in most brain regions tested, with levels that exceed 10% of β-actin levels in some brain regions (Figure 1) – an amazingly high expression level for a synaptic regulator! Cerebellin expression exhibited diverse patterns of developmental dynamics in different brain regions, ranging from developmentally constant levels to increasing or decreasing levels over the life of an animal (Figure 1). In general, Cbln2 was the most abundant, and Cbln4 the least abundant isoform, although in cerebellum Cbln1 exhibited increasing levels during development that reached extremely high values in adult mice, approaching 50% of β-actin levels.

Using the new genetic tools for monitoring Cbln2- and Cbln4-expressing neurons that we generated, we found that in adult mice, Cbln2 and Cbln4 were primarily expressed in diverse subsets of excitatory projection neurons, with occasional expression in inhibitory neurons (such as Cbln2-expressing inhibitory neurons in the main and accessory olfactory bulb and in the ventrolateral suprachiasmatic nucleus; Figures 4–9). Cbln2 expression was particularly abundant in cortical neurons, granule and periglomerular neurons of the olfactory bulb, and some thalamic nuclei, whereas Cbln4 was highly expressed in mitral cells of the olfactory bulb and entorhinal cortex projection neurons. Interestingly, some classes of neurons were devoid of detectable Cbln2 and Cbln4 expression. For example, the vast majority of hippocampal CA1 and CA3 pyramidal neurons contained no Cbln2 or Cbln4 expression signal, even though subsets of cortical neurons abundantly expressed Cbln2 and Cbln4 (Figure 6, 7). Although Cbln2 and Cbln4 were largely expressed in non-overlapping populations of neurons, co-expression was observed for example in mitral cells in the accessory (85% overlap) but not main olfactory bulb (0% overlap), the somatosensory cortex (20% overlap), and some thalamic nuclei, most significantly the parafasicular nucleus, where Cbln2 and Cbln4 were co-expressed in 100% of labeled neurons. Previous studies showed that Cbln1 is also highly expressed in the parafascicular nucleus, and similar to Cbln2 and 4, seems to also be expressed in all parafasicular neurons (Kusnoor et al., 2010). This makes the parafascicular nucleus likely the only nucleus in the brain where every neuron expresses Cbln1, Cbln2, and Cbln4.

The expression patterns we observed with the Cbln2 and Cbln4 knockin reporters likely accurately reflect the expression of the corresponding genes because we inserted the reporters into the 3′ untranslated regions of the Cbln2 and Cbln4 mRNAS, thus avoiding potential problems created by tagging proteins or by creating artificial exons encoding reporters. However, the expression patterns do not tell us how abundant Cbln2 and Cbln4 proteins are, nor do they reveal the localizations of these proteins. At first glance, the mRNA measurements and reporter expression patterns for Cbln2 and Cbln4 do not always seem to agree; in the hippocampus, we detected relatively low but still robust expression of Cbln2, whereas the reporter expression showed that Cbln2 is not detectably expressed in the CA1 to CA4 region of the hippocampus except for a few scattered cells (compare Figs. 1 and 7). However, the intensity of the Cbln2-mVenus signal was very strong, suggesting that this apparent discrepancy arises because Cbln2 is highly expressed in only a very small subset of hippocampal neurons, as seen in Fig. 7g. The functional significance of this selective expression will need to be explored in future research.

As a general pattern, Cbln2 and Cbln4 were often expressed in complementary nuclei within a given pathway. For example, in the olfactory bulb, Cbln2 expression was found in inhibitory PGCs and granule cells, which modulate the activity of excitatory mitral cells, while Cbln4 was expressed in the mitral cells. Given the fact that granule and mitral cells in the olfactory bulb are connected by reciprocal dendrodendritic synapses and that cerebellins are thought to act primarily presynaptically, Cbln2 and Cbln4 may have fundamental functions in shaping dendrodendritic synapses by controlling formation, function, and/or maintenance of the excitatory mitral → granule cell or the inhibitory granule → mitral cell subsynapse, an exciting possibility that illustrates the differential functions of these interesting proteins. Similarly, Cbln2 and Cbln4 were expressed in adjacent layers of the superior colliculus. Since that Cbln2 and Cbln4 may have distinct presynaptic receptors (neurexins vs. DCC), these complementary patterns suggest that differential activation of these receptors by Cbln2 and Cbln4 may contribute to synaptic specificity. Again, future experiments will test these interesting ideas.

References

Alberi L, Lintas A, Kretz R, Schwaller B, Villa AEP. The calcium-binding protein parvalbumin modulates the firing 1 properties of the reticular thalamic nucleus bursting neurons. Journal of Neurophysiology. 2013; 109:2827–2841. [PubMed: 23486206]

Alheid GF, Heimer L. New perspectives in basal forebrain organization of special relevance for neuropsychiatric disorders: the striatopallidal, amygdaloid, and corticopetal components of substantia innominata. Neuroscience. 1988; 27:1–39. [PubMed: 3059226]

Alonso A, Klink R. Differential electroresponsiveness of stellate and pyramidal-like cells of medial entorhinal cortex layer II. Journal of Neurophsiology. 1993; 70(1):128–143.

Arai R, Jacobowitz D, Deura S. Distribution of calretinin, calbindin-D28k, and parvalbumin in the rat thalamus. Brain Research Bulletin. 1994; 33(5):595–614. [PubMed: 8187003]

Bao D, Pang Z, Morgan MA, Parris J, Rong Y, Li L, Morgan J. Cbln1 is essential for interaction-dependent secretion of Cbln3. Molecular & Cellular Biology. 2006; 26:9327–9337. [PubMed: 17030622]

Born G, Schmidt M. A reciprocal connection between the ventral lateral geniculate nucleus and the pretectal nuclear complex and the superior colliculus: An *in vivo* characterization in the rat. Visual Neuroscience. 2008; 25:39–51. [PubMed: 18282309]

Boucard A, Ko J, Südhof TC. High affinity neurexin binding to cell adhesion G-protein-coupled receptor CIRL/latrophilin-1 produces an intercellular adhesion complex. Journal of Biological Chemistry. 2012; 287(12):9399–413. [PubMed: 22262843]

Bourgeron T. From the genetic architecture to synaptic plasticity in autism spectrum disorder. Nature Reviews Neuroscience. 2015; 16:551–563. [PubMed: 26289574]

Cagle M, Honig M. Parcellation of cerebellins 1, 2, and 4 among different subpopulations of dorsal horn neurons in mouse spinal cord. Journal of Comparative Neurology. 2014; 522:479–497. [PubMed: 23853053]

Chrobak JJ, Lörincz A, Buzsáki G. Physiological patterns in the hippocampo-entorhinal cortex system. Hippocampus. 2000; 10:457–465. [PubMed: 10985285]

Clarke R, Lee S, Eapen V. Pathogenetic model for Tourette syndrome delineates overlap with related neurodevelopmental disorders including Autism. Translational Psychiatry. 2012; 2:e158. [PubMed: 22948383]

DeFelipe J, Fariñas I. The pyramidal neuron of the cerebral cortex: morphological and chemical characteristics of the synaptic inputs. Progress in Neurobiology. 1992; 39:563–607. [PubMed: 1410442]

Dolorfo CL, Amaral DG. Entorhinal cortex of the rat: topographic organization of intrinsic connections. Journal of Comparative Neurology. 1998; 398:49–82. [PubMed: 9703027]

Frassoni C, Bentivoglio M, Spreafico R, Sánchez MP, Puelles L, Fairen A. Postnatal development of calbindin and parvalbumin immunoreactivity in the thalamus of the rat. Developmental Brain Research. 1991; 58:243–249. [PubMed: 2029767]

Friauf E. Distribution of calcium-binding protein calbindin-D28k in the auditory system of adult and developing rats. Journal of Comparative Neurology. 1994; 349:193–211. [PubMed: 7860778]

Haddick PC, Tom I, Luis E, Quinones G, Wranik BJ, Ramani SR, Stephen JP, Tessier-Lavigne M, Gonzalez LC. Defining the ligand specificity of the deleted in colorectal cancer (DCC) receptor. PLoS One. 2014; 9(1):e84823. [PubMed: 24400119]

Hayes TL, Lewis DA. Nonphosphorylated neurofilament protein and calbindin immunoreactivity in layer III pyramidal neurons of human neocortex. Cerebral Cortex. 1992; 2:56–67. [PubMed: 1633408]

Hirai H, Pang Z, Bao D, Miyazaki T, Li L, Miura E, Parris J, Rong Y, Watanabe M, Yuzaki M, Morgan J. Cbln1 is essential for synaptic integrity and plasticity in the cerebellum. Nature Neuroscience. 2005; 8(11):1534–1541. [PubMed: 16234806]

Hof PR, Glezer II, Conde F, Flagg RA, Rubin MB, Nimchinsky EA, Vogt Weisenhorn DM. Cellular distribution of the calcium-binding proteins parvalbumin, calbindin, and calretinin in the neocortex of mammals: phylogenetic and developmental patterns. Journal of Chemical Neuroanatomy. 1998; 16:77–116.

Huerta MF, Hartin JK. Connectional organization of the superior colliculus. Trends in Neuroscience. 1984; 7(8):286–289.

Ito T, Bishop DC, Oliver DL. Expression of glutamate and inhibitory amino acid vesicular transporters in the rodent auditory brainstem. Journal of Comparative Neurology. 2011; 519:316–340. [PubMed: 21165977]

Ito-Ishida A, Miura E, Emi K, Matsuda K, Iijima T, Kondo T, Kohda K, Watanabe M, Yuzaki M. Cbln1 regulates rapid formation and maintenance of excitatory synapses in mature cerebellar Purkinje cells *in vitro* and *in vivo*. Journal of Neuroscience. 2008; 28(23):5920–5930. [PubMed: 18524896]

Jacobowitz D, Winsky L. Immunocytochemical localization of calretinin in the forebrain of the rat. Journal of Comparative Neurology. 1991; 304:198–218. [PubMed: 2016417]

Jones EG, Hendry SHC. Differential calcium binding protein immunoreactivity distinguishes classes of relay neurons in monkey thalamic nuclei. European Journal of Neuroscience. 1989; 1(3):222–245. [PubMed: 12106154]

Kay LM, Freeman WJ. Bidirectional processing of olfactory-limbic axis during olfactory behavior. Behavioral Neuroscience. 1998; 112(3):541–553. [PubMed: 9676972]

Kishore U, Gaboriaud C, Waters P, Shrive A, Greenhough T, Reid K, Sim R, Arlaud G. C1q and tumor necrosis factor superfamily: modularity and versatility. TRENDS in Immunology. 2004; 25(10): 551–561. [PubMed: 15364058]

Kosaka K, Aika Y, Toida K, Heizmann CW, Hunzikar W, Jacobowitz DM, Nagatsu I, Streit P, Visser TJ, Kosaka T. Chemically defined neuron groups and their subpopulations in the glomerular layer of the rat main olfactory bulb. Neuroscience Research. 1995; 23:73–88. [PubMed: 7501303]

Kubota Y, Hattori R, Yui Y. Three distinct subpopulations of GABAergic neurons in rat frontal agranular cortex. Brain Research. 1994; 649:159–173. [PubMed: 7525007]

Kusnoor S, Parris J, Muly E, Morgan J, Deuth A. Extracerebellar role for *Cerebellin 1*: Modulation of dendritic spine density and synapses in striatial medium spiny neurons. Journal of Comparative Neurology. 2010; 518:2525–2537. [PubMed: 20503425]

Lee S, Uemura T, Yoshida T, Mishina M. GluRδ2 Assembles Four Neurexins into Trans-Synaptic Triad to Trigger Synapse Formation. Journal of Neuroscience. 2012; 32(13):4688–4701. [PubMed: 22457515]

Liu P, Jenkins N, Copeland N. A highly efficient recombineering-based method for generating conditional knockout mutations. Genome Research. 2003; 13:476–484. [PubMed: 12618378]

Lo F, Cork R, Mize R. Physiological properties of neurons in the optic layer of the rat's superior colliculus. Journal of Neurophysiology. 1998; 80:331–343. [PubMed: 9658054]

Lohmann C, Friauf E. Distribution of the calcium-binding proteins parvalbumin and calretinin in the auditory brainstem of adult and developing rats. Journal of Comparative Neurology. 1996; 367:90–109. [PubMed: 8867285]

Lu E, Llano D, Sherman S. Different distributions of calbindin and calretinin immunostaining across the medial and dorsal subdivisions of the mouse medial geniculate body. Hearing Research. 2009; 257:16–23. [PubMed: 19643174]

Matsuda K, Miura E, Miyazaki T, Kakegawa W, Emi K, Narumi S, Fukazawa Y, Ito-Ishida A, Kondo T, Shigemoto R, Watanabe M, Yuzaki M. Cbln1 is a ligand for an orphan glutamate receptor delta2, a bidirectional synapse organizer. Science. 2010; 328:363–368. [PubMed: 20395510]

Matsuda K, Yuzaki M. Cbln family proteins promote synapse formation by regulating distinct neurexin signaling pathways in various brain regions. European Journal of Neuroscience. 2011; 33:1447–1461. [PubMed: 21410790]

McDonald AJ. Cortical pathways to the mammalian amygdala. Progress in Neurobiology. 1998; 55:257–332. [PubMed: 9643556]

McDonald AJ, Mascagni F. Colocalization of the calcium-binding proteins and GABA in neurons of the rat basolateral amygdala. Neuroscience. 2001; 105:681–693. [PubMed: 11516833]

Miller A, Vedder L, Law L, Smith D. Cues, context, and long-term memory: the role of the retrosplenial cortex in spatial cognition. Frontiers in Human Neuroscience. 2014; 8:586. [PubMed: 25140141]

Miura E, Iijima T, Yuzaki M, Watanabe M. Distinct expression of Cbln family mRNAs in developing and adult mouse brains. European Journal of Neuroscience. 2006; 24:750–760. [PubMed: 16930405]

Molyneaux B, Arlotta P, Menezes J, Macklis J. Neuronal subtype specification in the cerebral cortex. Nature Neuroscience. 2007; 8:427–437. [PubMed: 17514196]

Naumann RK, Ray S, Prokop A, Las L, Heppner FL, Brecht M. Conserved size and periodicity of pyramidal patches in layer 2 of medial/caudal entorhinal cortex. Journal of Comparative Neurology. 2015; 524:783–806. [PubMed: 26223342]

Neville, KR., Haberly, LB. Olfactory cortex. In: Shepherd, GM., editor. The synaptic organization of the brain. Oxford University Press; 2004. p. 415-454.

Orona E, Rainer EC, Scott JW. Dendritic and axonal organization of mitral and tufted cells in the rat olfactory bulb. Journal of Comparative Neurology. 1984; 226:346–356. [PubMed: 6747027]

Otsuka S, Konno K, Abe M, Motohashi J, Kohda K, Sakimura K, Watanabe M, Yuzaki M. Roles of Cbln1 in non-motor functions of mice. Journal of Neuroscience. 2016; 36(46):11801–11816. [PubMed: 27852787]

Pang Z, Zuo J, Morgan J. Cbln3, a novel member of the precerebellin family that binds specifically to Cbln1. Journal of Neuroscience. 2000; 20:6333–6339. [PubMed: 10964938]

Potter G, Petryniak M, Shevchenko E, McKinset G, Ekker M, Rubenstein J. Generation of Cre-transgenic mice using *Dlx1/Dlx2* enhacers and their characterization in GABAergic interneurons. Molecular and Cellular Neuroscience. 2009; 40:167–186. [PubMed: 19026749]

Rong Y, Wei P, Parris J, Guo H, Pattarini R, Correia K, Li L, Kusnoor S, Deutch A, Morgan J. Comparison of Cbln1 and Cbln2 functions using transgenic and knockout mice. Journal of Neurochemistry. 2012; 120:528–540. [PubMed: 22117778]

Ryu K, Yokoyama M, Yamashita M, Hirano T. Induction of excitatory and inhibitory presynaptic differentiation by GluD1. Biochemical & Biophysical Research Communications. 2012; 417:157–161. [PubMed: 22138648]

Sah P, Faber E, Lopez de Armentia M, Power J. The amygdaloid complex: Anatomy and physiology. Physiological Reviews. 2003; 83:803–834. [PubMed: 12843409]

Santiago A, Shammah-Lagnado S. Efferent connections of the nucleus of the lateral olfactory tract in the rat. Journal of Comparative Neurology. 2004; 471:314–332. [PubMed: 14991564]

Sommer MA. The role of the thalamus in motor control. Current Opinion in Neurobiology. 2003; 13:663–670. [PubMed: 14662366]

Südhof TC. Neuroligins and neurexins link synaptic function to cognitive disease. Nature. 2008; 455:903–910. [PubMed: 18923512]

Sugar J, Witter M, van Strien N, Cappaert N. The retrosplenial cortex: intrinsic connectivity and connections with the (para)hippocampal region in the rat. An interactive connectome. Frontiers in Neuroscience. 2011; 5:7.

Uemura T, Lee SJ, Yasumura M, Takeuchi T, Yoshida T, Ra M, Taguchi R, Sakimura K, Mishina M. *Trans*-synaptic interaction of GluRδ2 and Neurexin through Cbln1 mediates synapse formation in the cerebellum. Cell. 2010; 141:1068–1079. [PubMed: 20537373]

Urade Y, Oberdick J, Molinar-Rode R, Morgan J. Precerebellin is a cerebellum-specific protein with similarity to the globular domain of complement C1q B chain. Proceedings of the National Academy of Science. 1991; 88:1069–1073.

van Groen T, Wyss JM. Connections of the retroplenial granular A cortex in the rat. Journal of Comparative Neurology. 1990; 300:593–606. [PubMed: 2273095]

Wei P, Pattarini R, Rong Y, Guo H, Bansal P, Kusnoor S, Deutch A, Parris J, Morgan J. The Cbln family of proteins interacts with multiple signaling pathways. Journal of Neurochemistry. 2012; 121:717–729. [PubMed: 22220752]

Wyss JM, van Groen T. Connections between the retrosplenial cortex and the hippocampal formation in the rat: A review. Hippocampus. 1992; 2(1):1–12. [PubMed: 1308170]

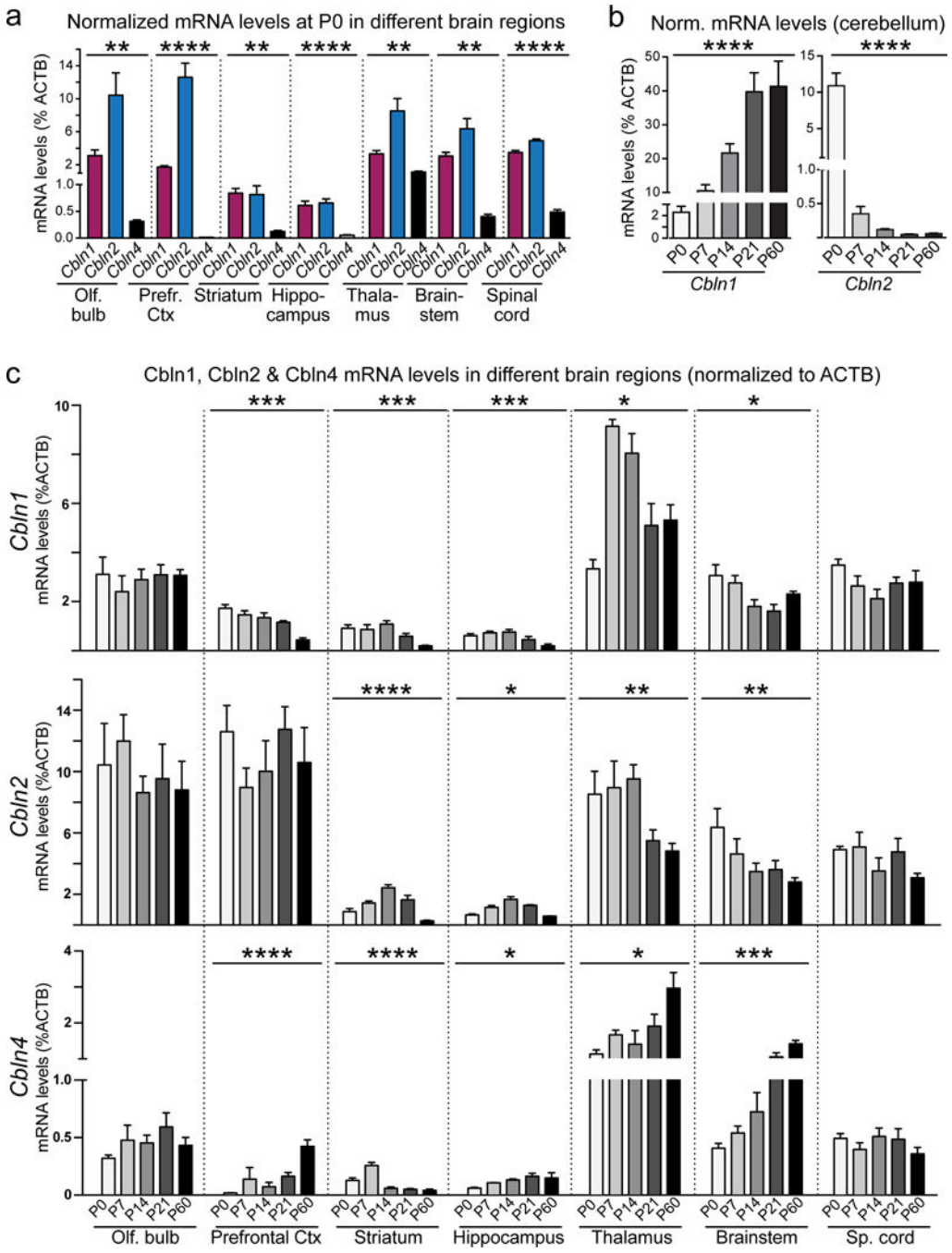

Figure 1. Differential developmental expression of Cbln1, Cbln2, and Cbln4 mRNAs in different mouse brain regions as analyzed by quantitative RT-PCR

A. Absolute levels of Cbln1, Cbln2, and Cbln4 mRNAs (relative to β-actin) in olfactory bulb, prefrontal cortex, striatum, hippocampus, thalamus, brainstem, and spinal cord in newborn mice at postnatal day 0 (P0). mRNAs were quantified in tissue lysates by RT-PCR. Note that the mRNA measurements were made with crudely dissected brain regions; the hippocampus, for example, includes surrounding structures such as the subiculum and not just the CA1-CA4 regions.

B. Cbln1 (*left*) and Cbln2 (*right*) mRNAs are expressed in opposite developmental patterns in mouse cerebellum. mRNAs were quantified in cerebellar lysates from mice at P0, P7, P14, P21, and P60; data show absolute mRNA levels relative to β-actin.
C. Systematic analysis of the expression of Cbln1 (top), Cbln2 (middle), and Cbln4 mRNAs (bottom) in olfactory bulb, prefrontal cortex, striatum, hippocampus, thalamus, brainstem, and spinal cord at P0, P7, P14, P21, and P60. mRNAs were quantified in lysates of the various brain regions, and first normalized to β-actin and then to the expression of the respective cerebellin isoform in the analyzed brain region at P0.
Data shown are means ± SEM (n = 6 mice). Asterisks denote statistical significance as assessed by one-way Kruskal-Wallis analysis of variance (ANOVA)(*$p \leq 0.05$, **$p \leq 0.01$, ***$p \leq 0.001$, ****$p \leq 0.0001$).

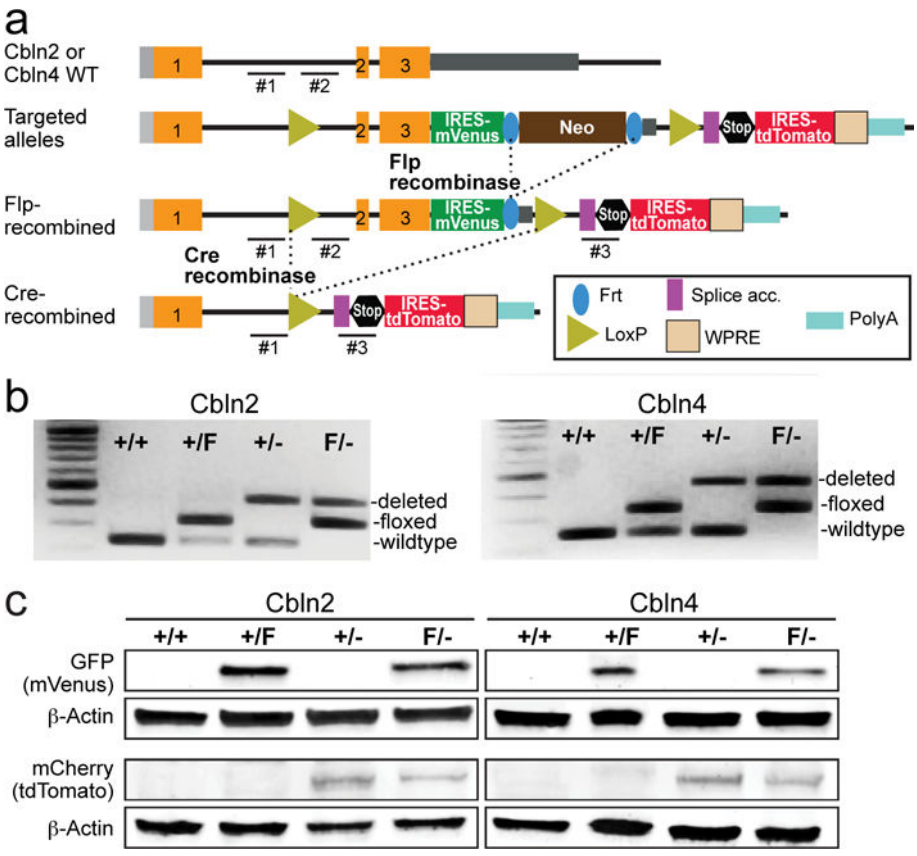

Figure 2. Design of Cbln2-mVenus-tdTomato and Cbln4-mVenus-tdTomato conditional knockin/knockout (cKO) mice

A. Schematic of the targeting strategy for generating Cbln2 and Cbln4 knockin/cKO mouse lines. For both cerebellins, the floxed exons 2 and 3 encode mVenus via an IRES sequence; Cre-mediated excision deletes most cerebellin coding sequences and IRES-mVenus expression, but activates IRES-mediated tdTomato expression.

B. PCR analysis of Cbln2 (left) and Cbln4 mutant genotypes (right). Forward primers were positioned upstream of the first LoxP site and reverse primers were positioned downstream of both LoxP sites, resulting in the following PCR product sizes for Cbln2: 225 bp (WT), 320 bp (Floxed), and 420 bp (KO); and for Cbln4: 234 bp (WT), 315 bp (Floxed), and 459 bp (KO).

C. Evaluation of validity of the genetic targeting strategy by immunoblotting of brain proteins from heterozygous Cbln2 knockin mice ($Cbln2^{+/flox}$; left) or heterozygous Cbln2 KO mice after Cre-mediated recombination ($Cbln2^{+/-}$; right). Samples were immunoblotted with antibodies to GFP (to detect mVenus) or mCherry (to detect tdTomato) and to actin (as a loading control). Note the abundant presence of mVenus only in the knockin mice and the weak expression of tdTomato only in the KO mice.

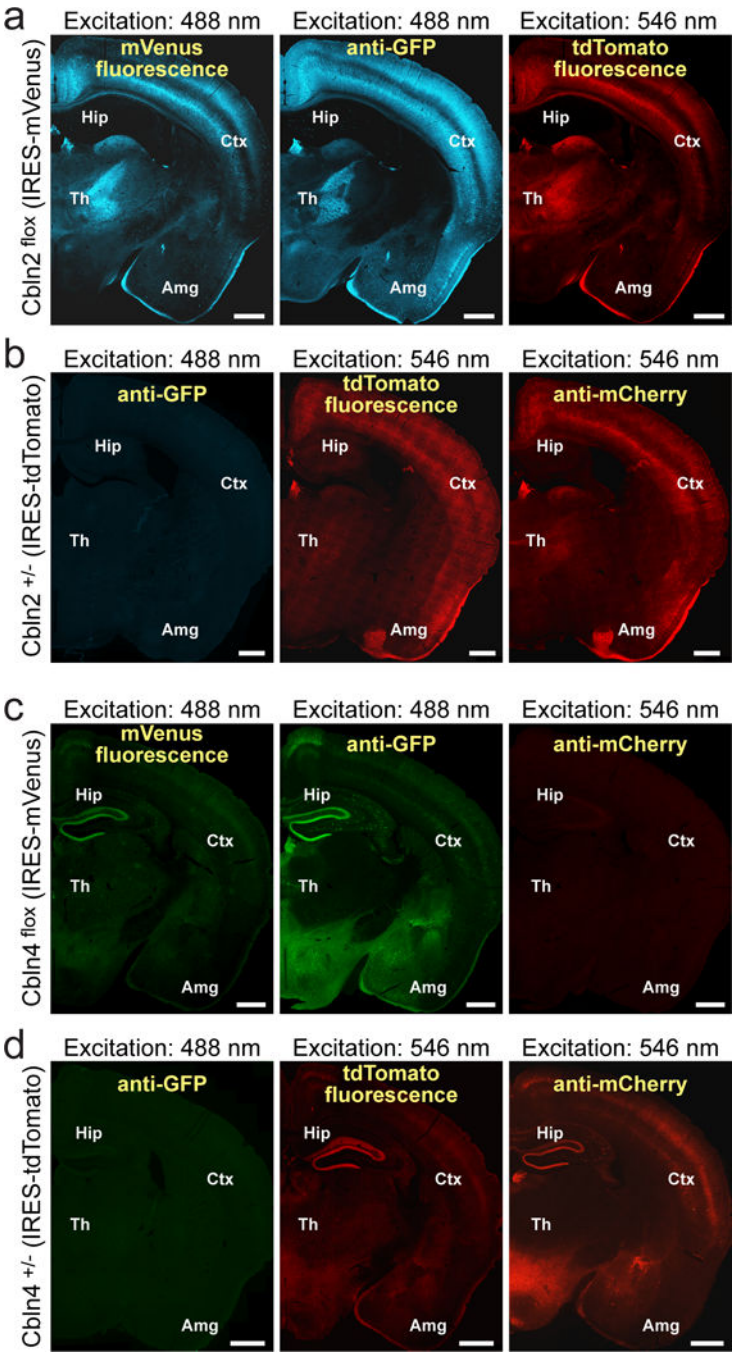

Figure 3. Immunocytochemical validation of the Cbln2-mVenus-tdTomato and Cbln4-mVenus-tdTomato conditional knockin and knockout mice

A & B. Test of the genetic targeting strategy by fluorescence microscopy of unstained or immunostained coronal sections from heterozygous Cbln2 knockin ($Cbln2^{+/flox}$; A) or Cbln2 KO mice ($Cbln2^{+/-}$; B). Sections were analyzed without staining to visualize endogenous mVenus (excitation 488 nm) or tdTomato signals (excitation 546 nm), or after immunostaining with GFP or mCherry antibodies (to detect mVenus and tdTomato, respectively), as indicated. Abbreviations used: Amg, amygdala; Ctx, cortex; Hip,

hippocampus; Th, thalamus. Apparent tdTomato fluorescence is visible in the absence of recombination, however, this is likely due to partial excitation of mVenus flourescence at 546 nm. Scale bars = 1 mm in all panels

C & ***D***. Same as A & B, except that sections from heterozygous Cbln4 knockin ($Cbln4^{+/flox}$; top) or KO mice ($Cbln4^{+/-}$; bottom) were analyzed. Note the precise correspondence between genetics and mVenus and tdTomato signals.

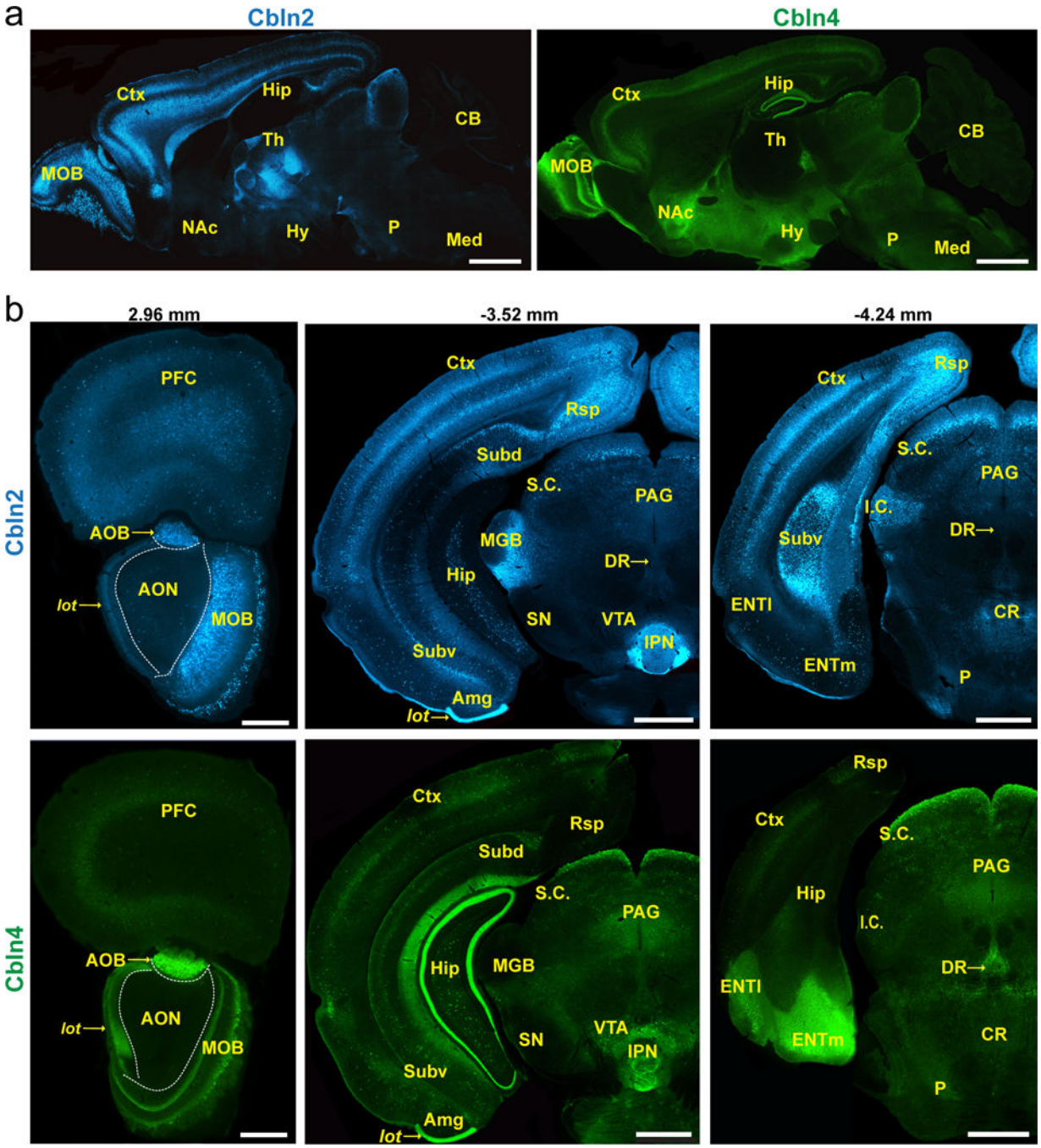

Figure 4. Overall expression patterns of Cbln2 (blue false colors) and Cbln4 (green false colors) throughout the adult mouse brain

A. Fluorescence microscopy images of sagittal sections (25 μm) of entire brains (lateral to medial sectioning orientation) from Cbln2$^{+/flox}$ (blue) or Cbln4$^{+/flox}$ mice (green) at P21. Sections were imaged via immunostaining for GFP. Note the restricted differential expression patterns of both cerebellins.

B. Same as A, except that coronal sections were examined (rostral to caudal sectioning orientation). Values above image denote the anteroposterior position of the section from Bregma in millimeters, based on Paxinos and Franklin (2001).
Scale bars = 1 mm in all images except for the 2.96 mm from Bregma images, where they are 0.5 mm. Abbreviations: Amg=amygdala; AOB=accessory olfactory bulb; AON=anterior olfactory nucleus; CB=cerebellum; CR=central raphe; Ctx=cortex; DR= dorsal raphe; ENTl=lateral entorhinal cortex; ENTm=medial entorhinal cortex; Hip=hippocampus; Hy=hypothalamus; I.C.=inferior colliculus; IPN=interpeduncular nucleus; *lot*=lateral olfactory tract; Med=medulla; NAc=nucleus accumbens; MGB=medial geniculate body; MOB=main olfactory bulb; P=pons; PAG=periaqueductal gray; PFC=prefrontal cortex; Rsp=retrosplenial cortex; S.C.=superior colliculus; Subd=dorsal subiculum; Subv=ventral subiculum; SN=substantia nigra; Th=thalamus; and VTA=ventral tegmental area

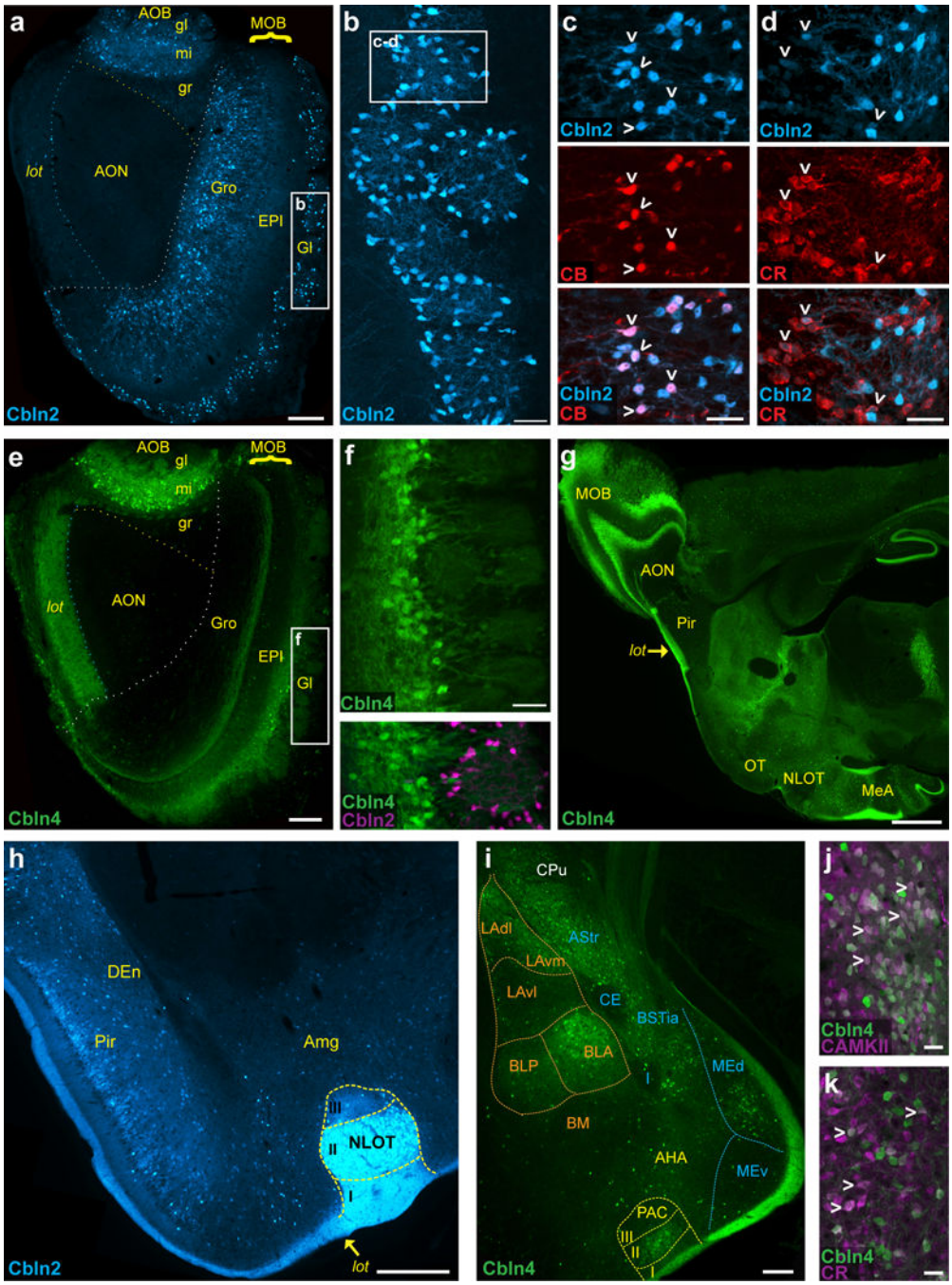

Figure 5. Cbln2 and Cbln4 are differentially expressed in olfactory brain regions

A. Cbln2 expression in the glomerular (Gl) and granule cell (GrO) layers of the main olfactory bulb (MOB), and in the mitral cell (mi), glomerular (gl), and granule cell (gr) layers of the accessory olfactory bulb (AOB).

B. High magnification image showing Cbln2 expression in the periglomerular cells (PGCs) of glomeruli in the main olfactory bulb (MOB).

C-D. Double labeling of Cbln2^{+} (blue) periglomerular cells with calbindin (CB; red; *C*), or calretinin (CR; red; *D*).

E. Cbln4 expression in the glomerular layer of the main olfactory bulb and the mitral cell layer of the accessory olfactory bulb.

F. High magnification image showing Cbln4 expression in mitral cells of the glomerular layer of the main olfactory bulb (*top*), and non-overlapping expression of Cbln4 in mitral cells (green) and Cbln2 in periglomerular cells (red; *bottom*).

G. Sagittal section showing Cbln4$^+$ mitral cell fibers exiting the MOB though the lateral olfactory tract (*lot*), and terminating in the medial amygdalar nucleus (MeA).

H. Cbln2$^+$ cell bodies in the olfactory-related piriform (Pir) and endopiriform (DEn) cortices, and in layer 2 of the nucleus of the lateral olfactory tract (NLOT) in the amygdala. The white arrow indicates Cbln2$^+$ fibers traveling from NLOT and forming part of the lateral olfactory tract (*lot*).

I. Expression of Cbln4 in the olfactory nuclei of the amygdala. Cbln4+ cell bodies are seen in the periamygdaloid complex (PAC), amygdalostriatal transition area (AStr), intra-amygdaloid subdivision of the BNST (BNSTia), posterior dorsal division of the medial nucleus (MEd), dorsolateral (LAdl) and ventromedial (LAvm) subdivisions of the lateral nucleus, and anterior division of the basolateral nucleus (BLA).

J. High magnification image of Cbln4$^+$ neurons (green) co-labeled with a CAMKII antibody (red) in the BLA.

K. High magnification image of Cbln4$^+$ neurons (green) co-labeled with calretinin (red) in the MEd. Arrowheads indicate colocalization of neurons.

Scale bars = 2 mm (*G*); 1 mm (*H, I*); 200 μm (*A, E*); 100 μm (*J, K*); 50 μm (*B, F*); and 25 μm (*C, D*). Bregma = 3.56 mm (*A, E*); −0.58 (*H*); and −1.82 mm (*I*). Additional abbreviations: AHA=anterior hypothalamic area; Amg=amygdala; AON=anterior olfactory nucleus; BLP=posterior basolateral nucleus; BM=basomedial nucleus; CE=central nucleus; I=intercalated nucleus; LAvl=ventral lateral division of lateral nucleus; MEv= ventral division of the medial nucleus; and OT=olfactory tubercle. Figure *G* shows a sagittal section; all other figures show coronal sections.

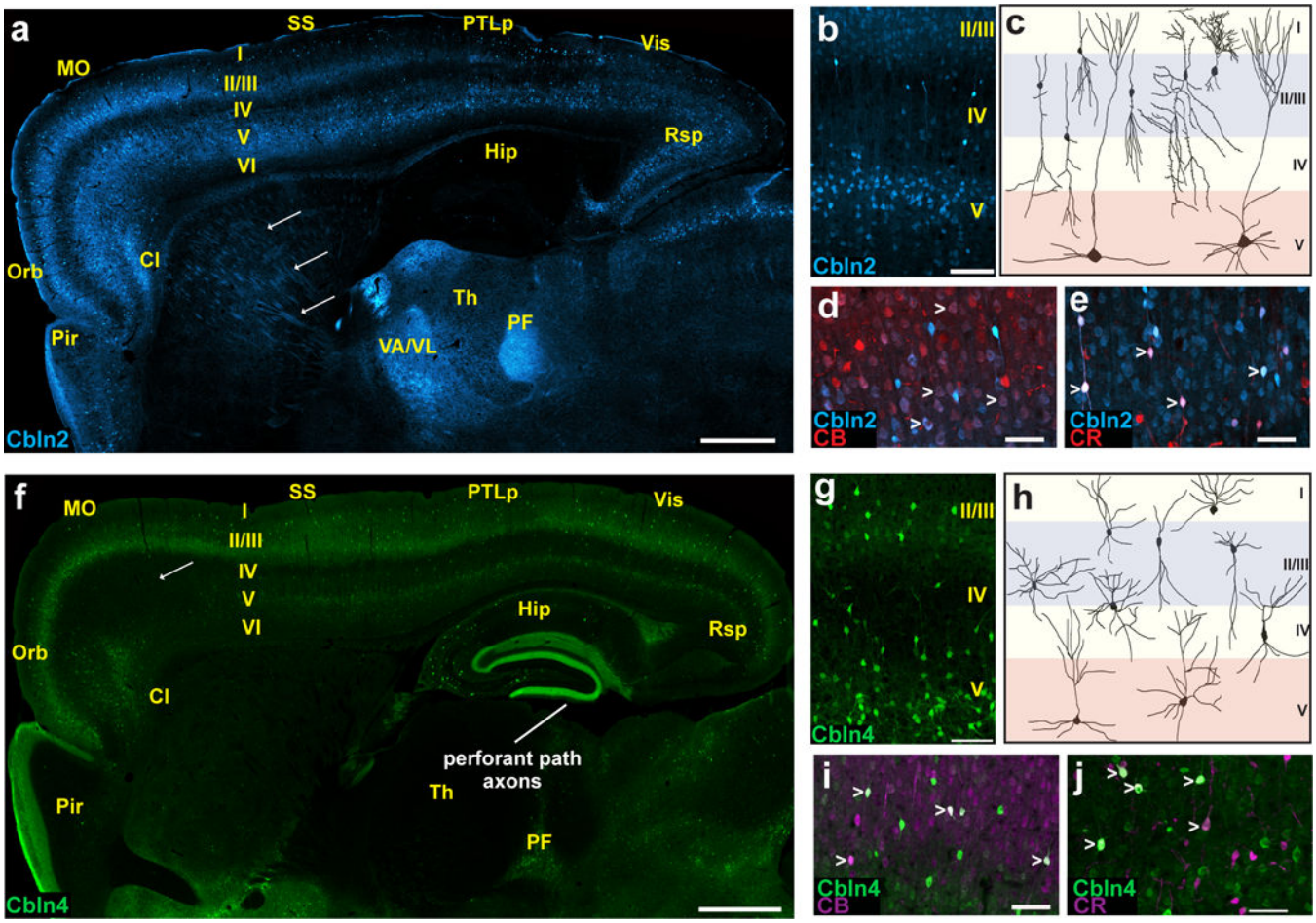

Figure 6. Expression profile of Cbln2 and Cbln4 in the cerebral cortex

A. Sagittal section from a Cbln2$^{+/flox}$ mouse visualized via staining with GFP antibody (arrows = Cbln2^{+} fibers extending from layer V of the motor cortex (MO) into the dorsal striatum).

B. Somatosensory cortex section illustrating Cbln2+ neurons in layers 2/3 and 5.

C. Neuron traces showing the morphology of Cbln2+ neurons in somatosensory cortex.

D & ***E***. Partial co-localization of Cbln2+ neurons (blue) with calbindin (CB; red; *D*) or calretinin (CR; red; *E*) in layers 2/3 of the somatosensory cortex (arrowheads identify selected double-labeled neurons).

F-J. Same as A-E, but for sections from Cbln4$^{+/flox}$ mice stained for GFP.

Scale bars = 2 mm (*A, F*); and 100 μm (*B, D, E, G, I, J*). Abbreviations for anatomical features: I, II/III, IV, V, and VI = corresponding cortical layers; Cl = claustrum; Hip=hippocampus; MO = motor cortex; Orb= orbital frontal cortex; PF=parafasicular thalamus; Pir = piriform cortex; PTLp = posterior parietal association cortex; Rsp= retrosplenial cortex; SS = primary somatosensory cortex; Th=thalamus; VA=ventral anterior; Vis = visual cortex; and VL= ventrolateral. Figures *A* and *F* show sagittal sections; all other figures show coronal sections.

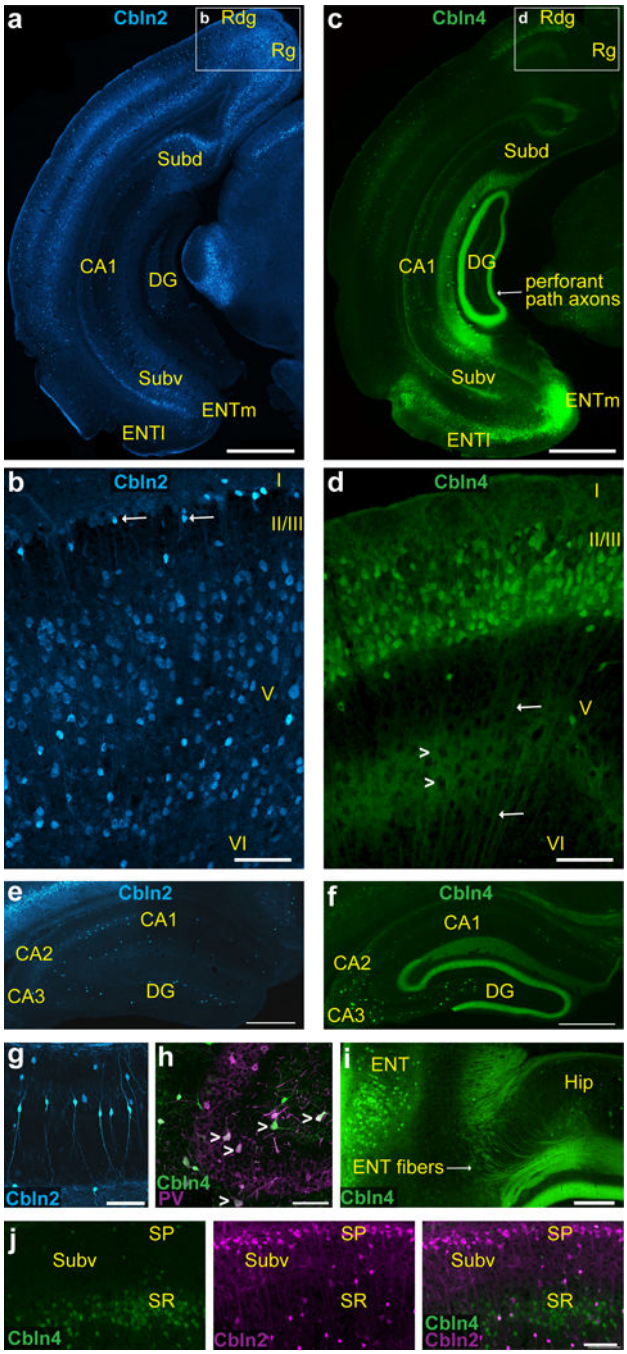

Figure 7. Expression of Cbln2 and Cbln4 in the retrosplenial cortex and hippocampal formation

A. Shows significant Cbln2 expression in the dysgranular (Rdg) and granular (Rg) retrosplenial cortex, and in the dorsal (Subd) and ventral (Subv) subiculum.

B. Higher magnification image of Rdg showing sparse labeling of Cbln2+ neurons in layers 2/3 (arrows) and dense labeling in layer 5.

C. Cbln4+ neurons are seen in Rdg, but not in Rg. Cbln4+ neurons are also seen in Subv, and in layer 2/3 of the lateral (ENTl) and medial (ENTm) entorhinal cortex (ENT). Cbln4+

axons from ENT are seen in the stratum lacunosum moleculare (perforant path axons; white arrow) of dentate gyrus (DG) and CA1 hippocampus.

D. Higher magnification image of Rdg showing densely populated Cbln4+ neurons in layer 2/3. Cbln4+ axons from these neurons can be seen traveling down (white arrows) into the corpus callosum. Cbln4+ neuropil can also be seen layer 5 (arrow heads).

E. Shows sparse labeling of Cbln2+ neurons in CA1, CA2, CA3 and DG hippocampus.

F. Same as E, but for Cbln4 expression.

G. High magnification image showing Cbln2+ neurons in CA1 hippocampus.

H. High magnification image showing Cbln4+ neurons co-labeled with parvalbumin (PV) in CA3 hippocampus.

I. Sagittal section showing Cbln4+ neurons in ENT and their axons traveling into the hippocampus (white arrow).

J. Co-labeling of Cbln2$^{+/-}$-tdTomato; Cbln4$^{+/F}$-mVenus sections showing Cbln4+ (green) neurons in the stratum radiatum (SR) and Cbln2+ (red) neurons in the pyramidal cell layer (SP) of Subv.

Scale bars = 2 mm (*A, C*); 500 um (*E-F*); 200 μm (*B, D, H, I*); and 100 μm (*G*). Bregma = −1.46mm (*E-F);* −4.10 mm (*A-D, I*). Except for *I*, all images show coronal sections.

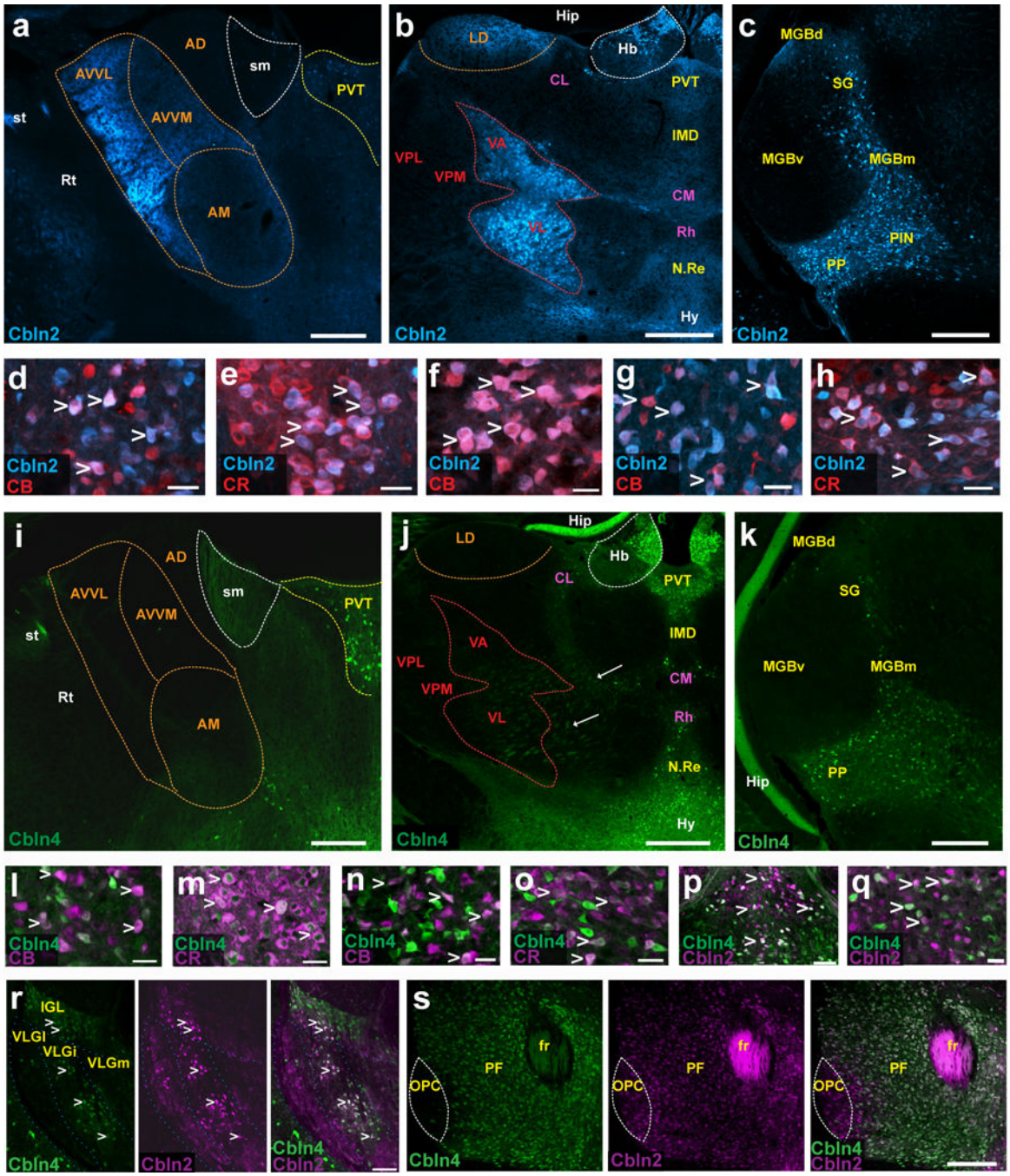

Figure 8. Differential expression of Cbln2 and Cbln4 in the thalamus and surrounding structures

A. Cbln2^{+} neurons in the paraventricular nucleus (PVT), and Cbln2^{+} neuropil in the ventrolateral subdivision of the anteroventral nucleus (AVVL).

B. Cbln2^{+} neurons in the ventrolateral (VL), ventral anterior (VA), paraventricular (PVT), intermediodorsal (IMD), central medial (CM), rhomboid (Rh), and reunions (Re) thalamic nuclei, and Cbln2^{+} neuropil in the lateral dorsal (LD) nucleus.

C. Cbln2^{+} neurons in the dorsal (MGBd) and medial (MGBm) subdivisions of the medial geniculate body (MGB), and in the related paralaminar nuclei (suprageniculate (SG), posterior intralaminar (PIN), and peripeduncular (PP) nuclei).
D & E. High magnification images of PVT neurons co-expressing Cbln2 (blue) and calbindin (CB; red; *D*) or calretinin (CR; red; *E*).
F. High magnification image of VL neurons co-expressing Cbln2 (blue) and CB (red).
G & H. Cbln2^{+} (blue) neurons in PIN co-labeled with either CB (red; *G*) or CR (red; *H*).
I. Cbln4+ neurons in the central portion of PVT.
J. Cbln4^{+} neurons in PVT, IMD, CM, Rh, Re, central lateral (CL), and paracentral (PCN) thalamic nuclei.
K. Cbln4^{+} neurons in MGBd, MGBm, SG, PIN, and PP.
L & M. High magnification image of PVT neurons co-expressing Cbln4 (green) and CB (red; *L*) or CR (red; *M*).
N & O. High Magnification image of PIN neurons co-expressing Cbln4 (green) and CB (red; *N*) or CR (red; *O*).
P. Co-labeling of Cbln2$^{+/-}$-tdTomato (red) and Cbln4$^{+/F}$-mVenus (green) in the PVT.
Q. Sparse co-labeling of PIN neurons for both Cbln4^{+} (green) and Cbln2^{+} (red).
R. Cbln4^{+} (green) neurons are seen in the intergeniculate leaflet (IGL) and intermediate (VLGi) lamina of the ventral lateral geniculate nucleus (*left*), and Cbln2^{+} (red) neurons are seen in IGL, VLGi, and the lateral lamina (VLGl; *center*). Neurons co-expressing both Cbln4 and Cbln2 are seen in the IGL and VLGi (*right*).
S. Robust Cbln4 (green) expression is seen throughout the parafasicular nucleus (PF), but is absent from the oval paracentral nucleus (OPC; *left*). Cbln2^{+} (red) neurons are seen throughout PF and OPC (*middle*), and all of the labeled PF neurons were both Cbln4^{+} and Cbln2^{+} (*right*).
Scale bars = 500 μm (*B, G, J, L*); 200 μm (*A, F, O*); 100 μm (*D, P*); and 25 μm (*C, E, H, I, K, M, N*). Bregma = −0.70 mm (*A, F*); −1.46 mm (*B, C, E, G-I*); −2.30 mm (*O, P*); and −2.92 mm (*J-N*). Additional abbreviations: AVVM = anteroventral nucleus, ventromedial subdivision; fr = fasciculus retroflexus; Hb = habenula; Hip=hippocampus; Hy=hypothalamus; sm = stria medullaris; and st = stria terminalis. All images show coronal sections.

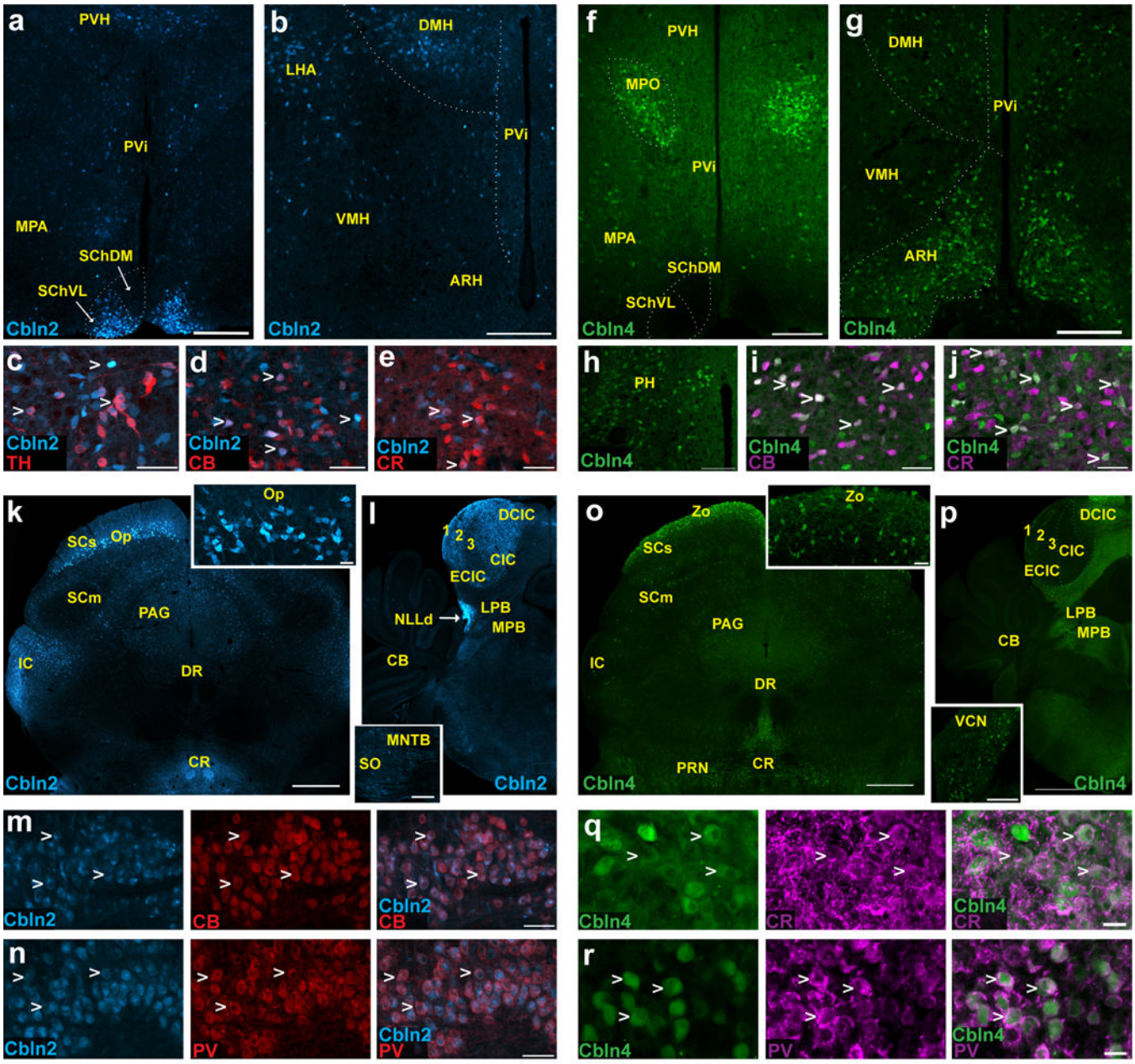

Figure 9. Expression of Cbln2 and Cbln4 in hypothalamic, midbrain, and hindbrain nuclei

A-D. Expression of Cbln2 in the hypothalamus. ***A.*** Cbln2+ neurons are seen in the periventricular (PVi) and paraventricular (PVH) hypothalamic nuclei, and in the ventrolateral subdivision of the suprachiasmatic nucleus (SChVL). ***B.*** Shows Cbln2+ neurons in PVi, as well as in the lateral hypothalamic area (LHA), and dorsomedial hypothalamic nucleus (DMH). ***C.*** Co-localization of Cbln2+ neurons (blue) and tyrosine hydroxylase+ neurons (TH; red) in PVH. ***D.*** Co-localization of Cbln2+ neurons (blue) with calbindin+ neurons (CB; red; *left*) or calretinin+ neurons (CR; red; *right*) in DMH. ***E-G.*** Cbln4 expression in the hypothalamus. ***E.*** Shows Cbln4+ neurons in the medial preoptic nucleus (MPO) and medial preoptic area (MPA). ***F.*** Shows Cbln4+ neurons in

DMH and PVi, as well as in the arcuate hypothalamic nucleus (ARH). **G.** Shows Cbln4+ neurons in the posterior hypothalamic area (PH), and co-localization of Cbln4+ neurons (green) with CB+ (red; *middle*) or CR+ neurons (red; *right*).

H. Cbln2+ neurons are seen in the inferior colliculus (IC), the optic layer (Op) of the sensory superior colliculus (SCs), throughout the motor SC (SCm), and in the periaqueductal gray (PAG). The boxed area shows a high magnification image of $Cbln2^+$ neurons in Op.

I. $Cbln2^+$ cell bodies are seen in layers 1 and 2, but not 3, of the external cortex (ECIC), the central nucleus (CIC), and the dorsal cortex of the inferior colliculus (DCIC). $Cbln2^+$ cell bodies are also seen in the dorsal division of the nucleus of the lateral lemniscus (NLLd), and the lateral parabrachial nucleus (LPB). The boxed area shows the superior olivary complex (SOC) and the medial nucleus of the trapezoid body (MNTB).

J & K. High magnification images showing $Cbln2^+$ (blue) neurons in the MNTB co-labeled with either CB (red; ***J***) or parvalbumin (PV; red; ***K***).

L. Shows Cbln4+ neurons in the zonal layer (Zo) of SCs, and in the SCm, PAG, pontine reticular nucleus (PRN) and central (CR) and dorsal raphe (DR). The boxed area shows a high magnification image of $Cbln4^+$ neurons in Zo.

M. Shows Cbln4+ neurons in the LPB and medial parabrachial nucleus (MPB). A few scattered Cbln4+ cell bodies were observed in layer 1 of ECIC, and in DCIC, but in no other regions of IC. The boxed area shows $Cbln4^+$ neurons in the ventral cochlear nucleus (VCN).

N-O. High magnification images showing $Cbln4^+$ (green) neurons in VCN co-labeled with either CR (red; ***N***) or PV (red; ***O***).

Arrowheads indicate co-labeled neurons in all. Scale bars = 500 μm (*H, I, L, M*); 200 μm (*A, B, E, F*, and the pull out in *I, M*); 100 μm (*G left*); 50 μm (*C, D, G middle and right, J, K*); and 20 μm (*N, O*). Bregma = −0.46 mm (*A, C, E*); −2.06 mm (*B, D, F*); −2.30 mm (*G*); −4.36 mm (*H, L*); and −4.96 mm (*I-K, M-O*). All images show coronal sections.

Table 1

List of primary antibodies.

Antigen	Immunogen	Manufacturer (Catalog #)	Species	Dilution	RRID #
Calbindin (CB)	Bovine kidney calbindin-D, clone 6B-955	Sigma-Aldrich (C9848)	Mouse, monoclonal	1:200	AB_476894
Calretinin (CR)	Recombinant rat calretinin, clone 6B8.2	Millipore (MAB1568)	Mouse, monoclonal	1:200	AB_94259
CAMKII	Partially purified rat CaM Kinase II, α-subunit, clone 6G9	Millipore (MAB8699)	Mouse, monoclonal	1:250	AB_2067919
GFP	Purified recombinant green fluorescent protein	Aves Lab (GFP-1020)	Chicken, polyclonal	1:1000 (IHC) 1:500 (WB)	AB_10000240
mCherry	Purified recombinant mCherry protein	Südhof lab (755A)	Rabbit, polyclonal	1:1000 (IHC) 1:500 (WB)	
Parvalbumin (PV)	Frog muscle parvalbumin, clone PARV-19	Sigma-Aldrich (P3088)	Mouse, monoclonal	1:500	AB_477329
Somatostatin (SOM)	Synthetic somatostatin coupled to keyhole limpet hemocyanin	Immunostar (20067)	Rabbit, polyclonal	1:100	AB_572264
Tyrosine hydroxylase (TH)	Tyrosine Hydroxylase purified from PC12 cells, clone LNC1	Millipore (MAB318)	Mouse, monoclonal	1:500	AB_2201528

Table 2

Analysis of Cbln2 and Cbln4 expression throughout the brain. Observed levels of expression: ++++=high, +++=moderate, ++=weak, +=very weak, —=not detected. NO= no overlap was observed between the Cbln-expressing neuron and the indicated marker. E= excitatory, I=inhibitory.

	Cbln2					Cbln4				
Region	**Cell Type/E/I**	**Density/Intensity**	**Co-Labeling**			**Cell Type/E/I**	**Density/Intensity**	**Co-Labeling**		
Main Olfactory bulb			**Calbindin**	**Calretinin**	**Parvalb.**			**Calbindin**	**Calretinin**	**Parvalb.**
Glomerular Layer (Gl)	Periglomerular/I	++++/++++	60% (n=1594)	4% (n=1543)	NO	Mitral/E	++++/++++	–	–	–
Mitral Layer (Mi)	–					Mitral/E	++/++	–	–	–
Granule Layer (GrO)	Granule/I	++++/++++	–	–	–	–				
Accessory Olfactory Bulb										
Glomerular Layer	Periglomerular/I	++++/+++	–	–	–	–				
Mitral Layer	Mitral/E	++++/++++	–	–	–	Mitral/E	++++/++++	–	–	–
Granule Layer	Granule/I	++++/++++	–	–	–	–				
Somatosensory Cortex										
Lamina I	Fibers	++++/++++	**E:** 70%			Fibers	++++/+++	**E:** 35%		
Lamina II/III	Pyramidal/E			4%	NO	Pyramidal/E			5%	NO
	Interneurons/I	+++/++++	**I:** 0% (n=1,386)	(n=1,545)		Interneurons/I	+++/++++	**I:** 10% (n=1,386)	(n=993)	
Lamina IV	Pyramidal/E	++/+++	NO	NO	NO	Stellate/E	++/+++	23% (n=82)	14% (n=94)	NO
						Interneurons/I	++/+++			
Lamina V	Pyramidal/E	++++/++++	NO	NO	NO	Pyramidal/E	+++/+++	5% (n=670)	0% (n=566)	NO
						Interneurons/I	++/+++			
Lamina VI	Pyramidal/E	++/+++	NO	NO	NO	Pyramidal/E	++/+++			
Retrosplenial Ctx						Interneurons/I	++/+++			
Lamina I	Fibers					Fibers				
Lamina II/III	Pyramidal/E	++/+++				Pyramidal/E	++++/++++	8% (n=921)	NO	NO
Lamina V	Pyramidal/E	++++/++++				Neuropil	++++/+++			
Claustrum	Type I spiny/E	++++/++++	NO	NO	NO	–				
Piriform Cortex										
Lamina I	Fibers					–				

	Cbln2					Cbln4				
Region	**Cell Type/E/I**	**Density/Intensity**	**Co-Labeling**			**Cell Type/E/I**	**Density/Intensity**	**Co-Labeling**		
Lamina II	Pyramidal/E	++++/++++				–				
Endopiriform Cortex	Somata/E	++++/++++	NO	NO	NO	–				
Hippcampal Formation										
CA1	Pyramidal/E	++/++++	+	+	N/O	Pyramidal/E	+/+	++	++	51%
	Interneurons/I	++/++				Interneurons/I	+/+			(n=225)
CA3	Pyramidal/E	++/++	+	+	N/O	Pyramidal/E	++/++	++	++	60%
	Interneurons/I	++/++				Interneurons/I	++/++++			(n=350)
Dentate Gyrus	Polymorphic/I	++/+++	N/O	+	N/O	Polymorphic/I	++/+++	N/O	++	44%
Dorsal Subiculum	Pyramidal/E	++++/++++				–				(n=182)
Ventral Subiculum										
Pyramidal Cell Layer	Pyramidal/E	++++/++++				–				
Stratum Radiatum	Interneurons/I	++/++++				Interneurons/I	++++/+++			
Entorhinal Cortex										
Lamina II	–					Pyramidal/E	++++/++++	++++	NO	NO
						Stellate/E	++/++++			
Lamina III	–					Pyramidal/E	++++/++++	++	NO	NO
Amygdala										
Superficial Cortical-like										
Amygdalohippocampal Area	–					Pyramidal-like/E	++/+++	NO	NO	NO
Anterior Cortical Amygdala	Fibers					Pyramidal-like/E	++/+++	NO	NO	NO
Posterior Cortical Amygdala	Fibers					Fibers				
Nuc Lateral Olfactory Tract										
Lamina I	Fibers					–				
Lamina II	Pyramidal-like/E	++++/++++	–	–	–	–				
Periamygdaloid Complex										
Lamina I	–					Fibers				
Lamina II	–					Pyramidal-like/E	++++/++++	NO	NO	NO
Basolateral Nuclear										
Anterior Basolateral	–					Pyramidal-like/E	++++/++++	NO	NO	NO
Posterior Basolateral	–					Pyramidal-like/E	+/+++	NO	NO	NO

J Comp Neurol. Author manuscript; available in PMC 2017 December 07.

	Cbln2					Cbln4				
Region	**Cell Type/E/I**	**Density/Intensity**	**Co-Labeling**			**Cell Type/E/I**	**Density/Intensity**	**Co-Labeling**		
Basomedial Nucleus	−					Pyramidal-like/E	+/+++	NO	NO	NO
Lateral Nucleus										
Dorsolateral	−					Pyramidal-like/E	+++/++++	NO	NO	NO
Ventrolateral	−					Pyramidal-like/E	++/++++	NO	NO	NO
Ventromedial	−					Pyramidal-like/E	++++/++++	NO	NO	NO
Centromedial Nuclear										
Anterior Amygdaloid Area	−					MSN-like/I	+++/++++	NO	NO	NO
Amygdalostriatal Area	−					MSN-like/I	++++/++++	NO	NO	NO
BNST	−					MSN-like/I	+++/++++	NO	NO	NO
Intra-Amygdaloid BNST	−					MSN-like/I	++/++++	NO	NO	NO
IPACm	−					MSN-like/I	++/++++	NO	NO	NO
Dorsal Medial Nucleus	Fibers					MSN-like/I	+++/++++	NO	++	NO
Ventral Medial Nucleus	Fibers					Fibers				
Septal Nuclei										
Lateral	Somata	+/+				Somata	++/++			
Triangular	−					Somata	++/++			
Basal Ganglia										
Caudate-Putamen	Somata/I	+/+++				Somata/I	++/+++			
Olfactory Tubercle	Neuropil	+++/+++				−				
Nucleus Accumbens	−					Somata/I	+++/++++	NO	NO	NO
Globus Pallidus	Fibers					Somata/I	+++/+++	NO	NO	NO
Ventral Tegemental Area	−					Somata	+++/++++	41% (n=530)	37% (n=551)	NO
Thalamus										
Anterior Nuclear Group										
Anteroventral, ventral lateral	Neuropil	++++/++++				−				
Lateral dorsal	Neuropil	++++/++++				−				
Ventral Nuclear Group										
Ventral Anterior	Somata/E	++++/++++	−	−	−	−				
Ventrolateral	Somata/E	++++/++++	100%	−	−	−				

	Cbln2					Cbln4				
Region	**Cell Type/E/I**	**Density/Intensity**	**Co-Labeling**			**Cell Type/E/I**	**Density/Intensity**	**Co-Labeling**		
Medial Nuclear Group										
Submedial Nucelus	Neuropil	+++/+++				–				
Midline Nuclear Group										
Paraventricular	Somata/E	+++/++	61%	90%	–	Somata/E	++++/++++	38%	94%	–
Intermediodorsal	Somata/E	++/++	(n=462)	(n=351)		Somata/E	++/+++	(n=1,275)	(n=842)	
Reunions	Somata/E	+++/+++	68%	78%	–	Somata/E	++++/++++	53%	86%	–
Intralaminar Nuclear Group			(n=314)	(n=898)				(n=1,045)	(n=1,152)	
Central Lateral	–					Somata/E	++/+++			
Paracentral	Somata/E	+/+				Somata/E	++/+++			
Central Medial	Somata/E	++/+++				Somata/E	++/+++			
Rhomboid	Somata/E	++/++				Somata/E	+++/+++			
Intralaminar Combined			60%	53%	–			45%	65%	–
			(n=197)	(n=411)				(n=650)	(n=667)	
Parafasicular	Somata/E	++++/++	NO	NO	–	Somata/E	++++/++++	N/O	N/O	–
Oval Paracentral	Somata/E	++++/++++	NO	NO	–	–				
Lateral Nuclear Group										
Lateral Posterior	Neuropil	++++/++++				–				
Lateral Geniculate Body		++/++++								
Intergeniculate Leaflet	Somata		NO	+++	–	Somata	+++/++++	NO	+++	–
Ventral Lateral	Somata	+++/+++	–	+++	NO	Somata	+/+++	–	+++	NO
Ventral Intermediate	Somata	++++/++++	NO	+++	–	Somata	++++/++++	NO	+++	–
Medial Geniculate Body										
Dorsal (MGBd)	Somata/E	++/+++	79%	73%	–	Somata/E	+/++	59%	57%	–
			(n=177)	(n=117)				(n=75)	(n=96)	
Medial (MGBm)	Somata/E	+++/++++	52%	69%	–	Somata/E	+++/+++	45%	29%	–
			(n=249)	(n=346)				(n=69)	(n=134)	
Supragenículate (SGN)	Somata/E	++/+++	52%	66%	–	Somata/E	++/+++	53%	42%	–
			(n=300)	(n=270)				(n=83)	(n=108)	
Posterior Intralaminar (PIN)	Somata/E	++++/++++	51%	70%	–	Somata/E	++++/+++	32%	46%	–
			(n=1,095)	(n=909)				(n=564)	(n=836)	

J Comp Neurol. Author manuscript; available in PMC 2017 December 07.

	Cbln2					Cbln4				
Region	**Cell Type/E/I**	**Density/Intensity**	**Co-Labeling**			**Cell Type/E/I**	**Density/Intensity**	**Co-Labeling**		
Peripeduncular (PP)	Somata/E	++++/++++	70% (n=478)	73% (n=372)	−	Somata/E	++++/+++	30% (n=143)	45% (n=248)	−
MGB/Paralaminar Nuclei Combined		57%	70% (n=2,300)	− (n=2,014)			37%	45% (n=934)	− (n=1,422)	
Epithalamus										
Lateral habenula	Somata/E	+++/++++				−				
Medial habenula	Somata/E	++++/++++				Somata/E	++++/+++			
Hypothalamus										
Preoptic Nucleus										
Medial	−					Somata	++++/++++	+++	+++	
Median	−					Somata	+++/++++	+++	+++	
Medial Preoptic Area	Somata	++/+++				Somata	++/+++	+++	++++	
Paraventricular	Somata	+++/+++	+++	NO	−	−			++++	
Periventricular	Somata	++/++	++	++	−	Somata	++/++	++	+++	
Ventrolateral	Somata/E&I	++++/++++	NO	NO	−	−				
Lateral Hypothalamic Area	Somata	++/+++	++	+++	−	−				
Dorsomedial Hypothalamic	Somata	++++/+++	+++	+++	−	Somata	++/+++	++	++	
Ventromedial Hypothalamic	−					Somata	+/+++			
Posterior Hypothalamic	Somata	++/+				Somata	++++/++++	++++	++++	
Arcuate Hypothalamic	−					Somata	++++/++++	NO	NO	
Mammillary Nuclei										
Suprmammillary, medial	Somata/E	+++/++++				Somata/E	++/++			
Suprmammillary, lateral	Fibers					Somata	++/++			
Lateral Mammillary	Somata/E	++++/+++				−				
Medial Mammillary, lateral	Somata/E	++++/+++				−				
Tubermammillay	Somata/E	++/++++				−				
Midbrain										
Interpeduncular Nucleus	Fibers					Fibers				
Dorsal Raphe Nuclei (DR)										
Drosal (DRD)	−					Somata	+++/+++	++	++++	−

	Cbln2					Cbln4				
Region	**Cell Type/E/I**	**Density/Intensity**	**Co-Labeling**			**Cell Type/E/I**	**Density/Intensity**	**Co-Labeling**		
Ventral (DRV)	Somata	++/+	−	++	−	Somata	++++/++++	−	++++	−
Ventrolateral (DRVL)	Somata	++/+	+++	++++	−	Somata	+++/+++	+++	++++	−
Interfasicular (DRI)	Somata	+++/+	++++	++	−	Somata	++++/++++	++++	+++	−
Central Linear Raphe	Somata	++/+	++++	++	−	Somata	++++/++++	++++	+++	−
Paramedian Raphe	Somata	+++/+++	−	+++	−	−				
Median Raphe	Somata	+++/+++	−	++	−	Somata	+/+++	−	++++	−
Pedunculopontine Tegmental	−					Somata	++++/++++	−	−	−
Periaqueductal Gray	Somata	+++/++				Somata	++++/+++			
Superior Colliculus, Sensory										
Zonal Layer	Somata	++/+	NO	−	NO	Somata/I	++++/++++	NO	−	NO
Superficial Gray	−					Somata	++/++			
Optic Layer	Somata/E	++++/++++	++++	−	N/O	Somata	++/+++			
Superior Colliculus, Motor	Somata	++/+++				Somata	++/+++			
Inferior Colliculus (IC)										
External (ECIC)										
Lamina I	Somata/E	+++/++++	NO	NO	NO	Somata/I	++/++++	NO	++	NO
Lamina II	Somata/E	++++/++++	NO	NO	NO	−				
Central (CIC)	Somata/E	++++/++++	NO	NO	NO	−				
Dorsal (DCIC)	Somata/E	++++/++++	NO	NO	NO	Somata/I	++/++++	NO	++	NO
Pons										
Pontine Gray	−					Somata/E	++++/+++			
Superior Olivary Complex	Somata/E&I	+++/++	−	−	100%	−				
Nuc of the Lateral Lemniscus										
Dorsal (NLLd)	Somata/I	++++/++++				−				
Ventral (NLLv)	Somata/I	+++/+++				Somata	+++/++			
Parabrachial Nucleus										
Superior Lateral	Somata	++++/+++				−				
Dorsal Lateral	Somata	++++/+++				−				
Ventral Lateral	−					−				

	Cbln2					Cbln4				
Region	**Cell Type/E/I**	**Density/Intensity**	**Co-Labeling**			**Cell Type/E/I**	**Density/Intensity**	**Co-Labeling**		
External Lateral	−					Somata	++++/+++			
Central Lateral	−					Somata	+++/+++			
Medial	Somata	+++/++				Somata	++++/+++			
Principal Sensory Nucleus	Somata	++/++				Somata	++/++			
Motor Nucleus	−					Somata	++/++			
Medulla										
Ventral Cochlear Nucleus	−					Globular/E	++++/+++	NO	75%	100%
						Bushy/E			(n=230)	
Medial Nuc of Trapezoid Body (MNTB)	Somata	++++/++	100%	++	100%	−				
Spinal Nuc of Trigeminal	Somata	+++/++				Somata	++/++			

J Comp Neurol. Author manuscript; available in PMC 2017 December 07.

Table 3

Quantification of Cbln2/Cbln4 co-expression in various brain regions. For each brain region, the percentage of total labeled neurons (n) expressing Cbln2 only, Cbln4 only, or co-expressing Cbln2 and Cbln4 in double labeled heterozygous Cbln2$^{+/-}$-tdTomato; Cbln4$^{+/F}$-mVenus sections is shown.

Region	**Expression**			**Region**	**Expression**		
Accessory Olfactory	**Cbln2+Cbln4**	**Cbln2**	**Cbln4**	**Thalamus**	**Cbln2+Cbln4**	**Cbln2**	**Cbln4**
Mitral layer	85% (n=961)	9%	6%	Paraventricular	32% (n=951)	11%	57%
Somatosensory Cortex				Reunions	31% (n=1,135)	11%	57%
Lamina II/III	20% (n=2,410)	45%	35%	Combined Intralaminar	40% (n=658)	23%	37%
Lamina V	20% (n=2,881)	55%	25%	Parafasicular	100%		
Hippocampal Formation				*Lateral Geniculate*			
CA1	31% (n=380)	45%	24%	Intergeniculate Leaflet	35% (n=312)	17%	48%
CA3	17% (n=520)	29%	55%	Ventral Lateral	15% (n=185)	85%	0%
Dentate Gyrus	34% (n=204)	31%	34%	Ventral Intermediate	53% (n=333)	28%	19%
Hypothalamus				MGB/Paralaminar	24% (n=1,673)	34%	42%
Periventricular	13% (n=260)	45%	42%				
Dorsomedial Hypothalamic	12% (n=772)	23%	65%				